Impact of the clinically approved BTK inhibitors on the conformation of full-length BTK and analysis of the development of BTK resistance mutations in chronic lymphocytic leukemia.

Raji E. Joseph[#*a], Thomas E. Wales[#b], Sandrine Jayne, Robert G. Britton, D. Bruce Fulton[a], John R. Engen[b], Martin J. S. Dyer[c] and Amy H. Andreotti[*a]

[a]Roy J. Carver Department of Biochemistry, Biophysics and Molecular Biology, Iowa State University, Ames, IA 50011, USA.

[b]Department of Chemistry and Chemical Biology, Northeastern University, Boston, MA 02115, USA.

[c]The Ernest and Helen Scott Haematological Research Institute, Leicester Cancer Research Centre, College of Life Sciences, University of Leicester, Leicester LE1 9HN, UK.

[#]These authors contributed equally to this work

[*] Co-corresponding author emails: jraji@iastate.edu, amyand@iastate.edu

ABSTRACT

Inhibition of Bruton's tyrosine kinase (BTK) has proven to be highly effective in the treatment of B-cell malignancies such as chronic lymphocytic leukemia (CLL), autoimmune disorders and multiple sclerosis. Since the approval of the first BTK inhibitor (BTKi), Ibrutinib, several other inhibitors including Acalabrutinib, Zanubrutinib, Tirabrutinib and Pirtobrutinib have been clinically approved. All are covalent active site inhibitors, with the exception of the reversible active site inhibitor Pirtobrutinib. The large number of available inhibitors for the BTK target creates challenges in choosing the most appropriate BTKi for treatment. Side-by-side comparisons in CLL have shown that different inhibitors may differ in their treatment efficacy. Moreover, the nature of the resistance mutations that arise in patients appears to depend on the specific BTKi administered. We have previously shown that Ibrutinib binding to the kinase active site causes unanticipated long-range effects on the global conformation of BTK (Joseph, R.E., et al., 2020, https://doi.org/10.7554/eLife.60470). Here we show that binding of each of the five approved BTKi to the kinase active site brings about distinct allosteric changes that alter the conformational equilibrium of full-length BTK. Additionally, we provide an explanation for the resistance mutation bias observed in CLL patients treated with different BTKi and characterize the mechanism of action of two common resistance mutations: BTK T474I and L528W.

Keywords**:** BTK, Bruton's Tyrosine Kinase; BTK inhibitors; CLL, chronic lymphocytic leukemia; Ibrutinib; Acalabrutinib; Zanubrutinib; Tirabrutinib; Pirtobrutinib; Fenebrutinib; drug resistance; allostery; conformational equilibrium; HDX-MS, hydrogen/deuterium exchange mass spectrometry and NMR, Nuclear Magnetic Resonance.

52 Abbreviations: BTKi, BTK inhibitor; LKD, linker-kinase domain; CLL, chronic lymphocytic
53 leukemia; MCL, Mantle cell lymphoma; MZL, Marginal zone lymphoma; PRR, proline-rich
54 region; HDX-MS, hydrogen/deuterium exchange-mass spectrometry; NMR, Nuclear Magnetic
55 Resonance; WT, wild-type.
56
57
58

INTRODUCTION

Ibrutinib (IMBRUVICA®), has revolutionized the treatment of the B cell malignancy, CLL [1]. Ibrutinib is a covalent active site inhibitor of the multi-domain B-cell kinase, BTK (Fig. 1a), that was first approved by the FDA in 2013 [2]. Inhibition of BTK disrupts signaling downstream of the B-cell receptor (BCR), a pathway on which the survival of CLL cells are dependent [3, 4]. The success of Ibrutinib has spurred the development of other BTKi including the now clinically approved BTK inhibitors: Acalabrutinib (CALQUENCE®), Zanubrutinib (BRUKINSA®), Tirabrutinib/ONO-4059 (VELEXBRU®), Pirtobrutinib/LOXO-405 (JAYPIRCA®) and Orelabrutinib (HIBRUKA®) [5-9]. All of the clinically approved BTKi (with the exception of Pirtobrutinib) are covalent active site inhibitors that bind to BTK C481 residue within the kinase active site. Pirtobrutinib is currently the first and only clinically approved non-covalent BTK active site inhibitor [7].

While BTKi are highly effective in the treatment of CLL, they are also being used to treat other B-cell malignancies such as Mantle cell lymphoma (MCL), Waldenström's macroglobulinemia, Marginal zone lymphoma (MZL) and are being evaluated in the treatment of multiple sclerosis and rheumatoid arthritis [5, 10, 11]. The plethora of clinically approved BTKi along with several other promising candidates currently in clinical trials pose a new challenge with respect to patient treatment. We now need a way to assess the suitability of a given BTKi for a given patient or disease state. Indeed, recent clinical trial data comparing one BTKi to another indicate that BTKi differ in their effectiveness in treating various conditions [12-15]. While toxicity, specificity and other criteria are used in these clinical comparisons, a molecular level characterization of the interaction of the inhibitor with full-length BTK is lacking and could be key to understanding these differences. In our previous work, using high resolution structural

82 biology techniques such as Nuclear Magnetic Resonance (NMR) and Hydrogen Deuterium
83 Exchange Mass Spectrometry (HDX-MS), we have shown that some inhibitors (Ibrutinib) exert
84 unanticipated allosteric effects upon binding to BTK while others (Fenebrutinib) do not [16].
85 Ibrutinib binding to the BTK kinase active site leads to a shift in the conformational ensemble of
86 full-length BTK towards an open conformation where the regulatory SRC homology (SH3 and
87 SH2) domains are released from the 'back' surface of the kinase domain, disrupting the closed
88 autoinhibited conformation of the full-length protein (Fig. 1b, [16]). Allosteric conformational
89 changes upon drug binding have been shown to alter protein-ligand interactions in other systems
90 with functional consequences *in vivo* [17-19]. The full impact of the panel of currently approved
91 BTKi on the conformation of full-length BTK is not known.

92 Despite the success of BTKi in CLL, a recurring problem is the development of BTKi
93 resistance. Resistance typically develops in patients ~2 years after the start of BTK inhibitor
94 treatment [20]. Analysis of CLL patients that stop responding to BTKi has revealed that most
95 develop mutations within *Btk* or in the substrate of BTK: Phospholipase C gamma 2 (PLCγ2) [21-
96 23]. Interestingly, the specific resistance mutations that develop in *Btk* seem to be dependent on
97 the specific BTKi used [23-29]. While data available so far for the BTKi inhibitors Acalabrutinib,
98 Zanubrutinib, Tirabrutinib and Pirtobrutinib are low in number, there is an emerging trend (Fig.
99 1c,d). Perhaps not surprisingly, patients treated with the reversible inhibitor Pirtobrutinib do not
100 develop mutations in C481 (Fig. 1d). Instead, they develop other kinase active site mutations
101 including BTK T474I and L528W (Fig. 1c,d) [26]. In contrast, 90% or more of CLL patients
102 treated with Ibrutinib and Acalabrutinib develop mutations in BTK C481 (Fig. 1d, Supp. Table 1
103 [21, 23]). Substitution of C481 with serine is the most common resistance mutation found in these
104 patients [30]. While mutation of BTK C481 to residues other than serine have also been reported

105 (C481F/Y/R), they occur at a much lower frequency [31]. Additionally, other sites within BTK
106 such as T474 and L528 are rarely (if ever) mutated in Ibrutinib and Acalabrutinib-treated CLL
107 patients (Fig. 1d, Supp. Table 1, [21-24, 29 , 30, 32-34]). Surprisingly, BTK T474 and L528 are
108 frequently mutated in CLL patients treated with the covalent inhibitors Zanubrutinib and
109 Tirabrutinib (Fig. 1d, [24, 27, 28]). BTK T474I and L528W are found at almost equal or higher
110 frequency compared to C481S in these patients (Fig. 1d, Supp. Table 1, [24, 27, 28]). Moreover,
111 in Zanubrutinib-treated patients, the L528W mutation was often present together with C481S
112 mutation (on different alleles), and with the L528W mutation present at a higher allelic frequency
113 compared to C481S [28]. This mutational bias with respect to covalent BTKi is unexpected given
114 the shared mode of action across the panel of covalent inhibitors, and the reasons for these
115 differences are unclear. Additionally, the mechanism of action of the BTK T474I and L528W
116 mutations is not known. Given the development of T474I and L528W mutations in multiple CLL
117 patients treated with both covalent (Zanubrutinib and Tirabrutinib) and non-covalent
118 (Pirtobrutinib) BTK inhibitors, we focused on these BTK mutations and explore their mechanisms
119 of action.

120 Here, we probe the impact of four clinically-approved BTKi: Acalabrutinib, Zanubrutinib,
121 Tirabrutinib and Pirtobrutinib on the conformation of full-length BTK. We find that each of these
122 BTKi brings about a unique combination of changes in full-length BTK. Acalabrutinib,
123 Zanubrutinib and Tirabrutinib disrupted the autoinhibited conformation of full-length BTK
124 similarly to Ibrutinib but did so to varying degrees. Interestingly, Acalabrutinib and Tirabrutinib
125 altered the dynamics of the kinase G-helix, a region that has been previously characterized as the
126 PLCγ substrate docking site [35]. Pirtobrutinib on the other hand stabilized the compact
127 autoinhibited conformation of full-length BTK and is the first BTK inhibitor observed to do so.

128 Additionally, we probed the mechanism of action of the BTK resistance mutations T474I and
129 L528W. We show that the catalytically inactive BTK L528W mutant activated the SRC kinase
130 HCK and that this activation is dependent on the proline-rich region within BTK. The BTK T474I
131 mutation disrupted binding to Zanubrutinib, Tirabrutinib and Pirtobrutinib and likely evades the
132 action of these drugs due to reduced binding to these inhibitors. Furthermore, we provide an
133 explanation for the mutational bias observed in patients treated with different covalent BTKi. The
134 development of the C481S resistance mutation is dependent on the half-life of the inhibitor which
135 likely explains the low prevalence of the C481S resistance mutation in patients treated with the
136 covalent inhibitors Tirabrutinib and Zanubrutinib (which have a long half-life) as compared to
137 Ibrutinib and Acalabrutinib (which have a short half-life). Characterization of the interaction of
138 BTKi with full-length BTK allows us to better interpret clinical trial results and will help guide
139 the choice of BTKi to be used for treatment. Furthermore, understanding the mechanism of action
140 of resistance mutations allows us to develop treatment strategies that either prevent or delay
141 development of resistance mutations and ways to treat them when they arise.

142

143 RESULTS

144 *Assessing the impact of inhibitor binding on the isolated BTK linker kinase domain by NMR.*

145 To evaluate the impact of inhibitor binding on BTK, we first monitored its effect on the
146 conformation of the linker kinase domain (LKD) fragment of BTK (Fig. 1a). The catalytic kinase
147 domain of BTK can adopt an active or inactive conformation in solution and previous studies have
148 shown that inhibitor binding can stabilize one or more of these conformations [16]. The switch
149 from an inactive to an active kinase conformation involves changes in key structural elements
150 within the kinase domain. These changes include the inward movement of the C-helix from an
151 inactive 'αC out' to the active 'αC in' position, changes in the side chain rotamer conformation of
152 BTK W395, formation of a conserved BTK K430:E445 salt bridge and unfurling of the collapsed
153 activation loop, leading to the exposure of the conserved Y551 on the activation loop for
154 phosphorylation (Fig. 2a, [16]).

155 Crystal structures of the BTK kinase domain in complex with Acalabrutinib, Zanubrutinib,
156 Tirabrutinib or Pirtobrutinib are available and show that each of these BTK inhibitors stabilize the
157 kinase domain in an inactive conformation similar to that of Ibrutinib-bound BTK (Fig. 2b-f, [16,
158 36-38]). In all the inhibitor bound structures the C-helix is in the 'αC out' position and the
159 activation loop is collapsed into the kinase active site, burying the conserved BTK Y551 (Fig. 2b-
160 f). Moreover, superposition of these BTK/inhibitor complexes shows that the structures of the
161 kinase domain remains largely the same regardless of which inhibitor is bound (Fig. 2g). The
162 structure of the Tirabrutinib bound BTK is the only structure that shows a difference; the activation
163 loop in that complex adopts an alternative inactive loop conformation compared to the other
164 inhibitor bound structures (Fig. 2e,g).

165 Previous NMR and HDX-MS analysis of the interaction of BTK with a different panel of
166 active site inhibitors has shown that there are differences between the solution and crystal behavior
167 [16]. To test whether the BTK inhibitors Acalabrutinib, Zanubrutinib, Tirabrutinib and
168 Pirtobrutinib can stabilize an inactive BTK kinase conformation in solution as predicted by the
169 crystal structures, we evaluated the BTK inhibitor bound complexes by NMR. The LKD fragment
170 of BTK was isotopically labeled with ^{15}N and a ^{1}H-^{15}N TROSY-HSQC spectrum was obtained in
171 the presence or absence of the inhibitor (Fig. 3). We have previously shown that BTK W395 within
172 the linker region (L) that precedes the kinase domain provides a useful probe to monitor the
173 conformational state adopted by the kinase domain in solution [16, 39]. Assignments for the apo
174 BTK linker kinase domain, which adopts the active (αC in) conformation, show that the W395
175 indole ^{1}H resonates at 10.21 ppm in the ^{1}H-^{15}N TROSY-HSQC spectrum (Fig. 3, top panel, black
176 spectrum). An upfield shift in the BTK W395 side chain indole NH resonance is observed upon
177 Ibrutinib binding and is consistent with the outward movement of the C-helix (αC out), and
178 stabilization of the inactive kinase domain conformation by Ibrutinib (Fig.3, top panel, cyan
179 spectrum [16]).

180 Comparing the tryptophan indole region of the ^{1}H-^{15}N TROSY-HSQC spectra for the BTK
181 LKD inhibitor bound to Acalabrutinib, Zanubrutinib or Tirabrutinib with that of the apo BTK LKD
182 protein shows that W395 undergoes an upfield shift in the presence of inhibitor (Fig. 3), suggesting
183 that, like Ibrutinib [16] and consistent with the crystal structures, all of these inhibitors stabilize
184 the inactive kinase domain conformation in solution. Interestingly, the Tirabrutinib bound
185 spectrum shows several peaks corresponding to W395, suggesting that the Tirabrutinib-bound
186 BTK kinase domain is likely adopting multiple kinase conformations in solution. Additionally, the
187 magnitude of the upfield shift in W395 resonance is smaller in both the Tirabrutinib and

188 Zanubrutinib spectra (compared to Ibrutinib and Acalabrutinib), which may reflect a relatively
189 larger active state population in these samples.

190 In contrast to the covalent inhibitors, Pirtobrutinib causes a downfield shift in W395, which
191 might suggest that this inhibitor is stabilizing an active conformation of BTK (Fig. 3, bottom
192 panel). However, the fluorinated benzene ring in Pirtobrutinib, which is adjacent to the C-helix
193 and W395 in the Pirtobrutinib bound structure, may cause changes in the local environment of
194 W395 and thereby give rise to the unusual chemical shift change. Indeed, HDX-MS data (see
195 below) confirms the stabilization of the inactive kinase conformation by Pirtobrutinib. All W395
196 assignments in the WT BTK inhibitor bound spectra were confirmed by comparison to the
197 corresponding ^{1}H-^{15}N TROSY-HSQC spectra of BTK LKD W395A mutant bound to the
198 inhibitors (Supp. Fig. S1).

199

200 *Probing the effects of inhibitor binding on full-length BTK by HDX-MS.*

201 We next evaluated the impact of inhibitor binding on the conformation of full-length BTK
202 by HDX-MS. We have previously shown that HDX-MS can be used to probe conformational
203 changes in full-length BTK that are brought about by inhibitor binding [16]. The structure of the
204 full-length BTK protein in the autoinhibited conformation was recently solved [40]. However,
205 electron density for both the N-terminal PHTH domain and proline rich region is missing in this
206 structure, suggesting that the N-terminal region of BTK is dynamic. Indeed, CryoEM, SAXS and
207 solution data all indicate that the PHTH domain is highly dynamic and likely transiently contacts
208 multiple sites on the core SH3-SH2-kinase domain (Fig. 1b, [40]). Changes in deuterium
209 incorporation must therefore be mapped on the crystal structure of the SH3-SH2-kinase fragment

210 of BTK, which adopts a compact inactive autoinhibited conformation (Fig. 1b, [41]). Additionally,
211 our previous work [16] has shown that for the majority of the inhibitor complexes studied changes
212 in deuterium incorporation are rarely observed in the PHTH domain suggesting that the PHTH
213 domain dynamics are not affected by active site occupancy. Inhibitor binding typically leads to
214 decreased deuterium incorporation in peptides derived from the kinase active site due to
215 stabilization of this region in the presence of the bound inhibitor [16]. Additionally, inhibitors such
216 as Ibrutinib that have allosteric effects lead to an increase in deuterium incorporation in peptides
217 derived from the BTK SH3 and SH2 domains as well as the SH2-kinase linker, indicating a shift
218 away from the autoinhibited conformation [16].

219 Full-length BTK was mixed with Acalabrutinib, Zanubrutinib, Tirabrutinib or Pirtobrutinib
220 and subjected to HDX-MS analysis. Peptides that could be followed in each of the six experimental
221 conditions (apo, and inhibitor bound) were used for comparison (see Supplemental Datafile). Intact
222 mass analysis supports a single binding site on BTK for the covalent inhibitors similar to what has
223 been observed previously with Ibrutinib (Fig. 4a, [16]).

224 Acalabrutinib, Zanubrutinib, Tirabrutinib and Pirtobrutinib show decreased deuterium
225 incorporation in peptides derived from the kinase N-lobe and kinase activation loop similar to that
226 observed previously with Ibrutinib (Fig. 4b,c, Fig. 5a-e, [16]). This is consistent with the binding
227 of these inhibitors in the kinase active site and stabilization of the inactive kinase conformation
228 observed by NMR as well as in the crystal structures. Furthermore, we note that each of these
229 inhibitors induce allosteric effects. Binding of Acalabrutinib, Zanubrutinib and Tirabrutinib to
230 BTK causes increased deuterium incorporation in peptides derived from the SH3 domain
231 suggesting that the autoinhibited conformation of full-length BTK is destabilized (Fig. 4b,c, Fig.
232 5b-d). This is similar to what has been previously observed with Ibrutinib [16]. Additionally,

233 Acalabrutinib and Tirabrutinib showed increased deuterium incorporation in peptides derived from
234 the G-helix of the kinase domain, a region that has been previously identified as the PLCγ substrate
235 docking site (Fig. 4b,c, Fig. 5b-d, [35]). Taken together, Acalabrutinib, Zanubrutinib and
236 Tirabrutinib binding to BTK leads to hybrid conformations of full-length BTK, where the kinase
237 domain is stabilized in an inactive conformation and the regulatory domains are disrupted from
238 their autoinhibitory conformation. In stark contrast, Pirtobrutinib binding to BTK shows decreased
239 deuterium incorporation in peptides derived from the SH3 and SH2 domains, suggesting that
240 Pirtobrutinib stabilizes the compact, autoinhibited conformation of full-length BTK (Fig. 4b,c, Fig.
241 5e). To date, Pirtobrutinib is the only inhibitor that we have tested that uniformly stabilizes both
242 the kinase domain as well as the regulatory domains in the inactive autoinhibited conformation.
243 Thus, each BTK inhibitor causes unique changes in the overall conformation of full-length BTK
244 that is not readily predicted from crystal structures. We next turn our attention to the distinct
245 resistance mutations that arise upon treatment with the different BTK inhibitors.

246

247 *Probing the intrinsic effects of the BTK T474I and L528W mutations.*

248 BTK resistance mutations can potentially confer a selective advantage to cells in several
249 ways: by increasing the activity of the kinase, by changing the conformation/stability of the kinase
250 which in turn can alter protein-protein interactions, or by disrupting drug binding. To probe the
251 mechanism by which the BTK T474I and L528W mutations confer resistance to Zanubrutinib,
252 Tirabrutinib and Pirtobrutinib we first tested the impact of each mutation on the catalytic activity
253 of the kinase and then investigated the impact on the overall conformation of the protein by HDX-
254 MS and NMR.

255 To test the catalytic activity of the BTK mutants we set up *in vitro* kinase assays using
256 purified full-length WT and mutant BTK proteins. Kinase activity was monitored by following
257 phosphorylation on the activation loop Y551 by western blotting. The BTK T474I mutant shows
258 phosphorylation on Y551, however it is lower than that of the WT protein (Fig.6a,b) suggesting
259 that the T474I mutation reduces the activity of the kinase. In contrast, the BTK L528W mutant is
260 completely inactive with no detectable phosphorylation on Y551 throughout the time course
261 (Fig.6c,d). These results are consistent with previous activity reports on both the BTK T474I and
262 L528W mutants [26, 28, 42, 43]. Given that neither the BTK T474I or the L528W mutant had
263 increased catalytic activity, augmenting kinase activity is not the mechanism by which these
264 mutations confer resistance.

265 Resistance mutations can change the conformation of the protein which in turn can alter
266 protein-protein interactions. To test whether the BTK T474I and L528W mutations alter the overall
267 conformation of the protein, we carried out HDX-MS analysis on the apo mutant proteins.
268 Comparing the BTK T474I mutant to WT BTK, the BTK T474I mutant shows increased deuterium
269 incorporation within the kinase domain N-lobe β2-β3 strands and the activation loop, but no
270 changes elsewhere on the protein (Fig.6e,f,h). These increased dynamics within the N-lobe of the
271 BTK T474I mutant could potentially alter drug binding to the active site. The BTK L528W mutant
272 on the other hand shows a slight decrease in deuterium incorporation in the kinase domain and the
273 SH3 domain suggesting that the L528W mutation has a slight stabilizing effect on the full-length
274 autoinhibited conformation of BTK (Fig.6e,g,h).

275 Additionally, we tested the BTK T474I and L528W mutants by NMR. An overlay of the
276 ^{1}H-^{15}N TROSY-HSQC spectra of apo BTK LKD T474I with that of apo WT BTK LKD shows
277 some changes in the mutant spectrum (Fig.6i). The resonance corresponding to BTK A524 located

278 close (~18 Å) to T474 in the kinase active site shows line broadening in the BTK T474I mutant
279 spectrum suggesting increased dynamics in the mutant. This is consistent with the increased
280 deuterium incorporation observed in the kinase domain for this mutant by HDX-MS. The BTK
281 W395 resonance in the BTK T474I mutant spectrum overlaps with that of the WT suggesting that
282 the mutant kinase domain adopts an active conformation similar to that of the WT protein. The
283 BTK L528W mutant on the other hand shows a small upfield shift in the W395 resonance,
284 suggesting that the BTK L528W mutant kinase domain is shifted slightly towards an inactive
285 conformation compared to the WT protein. This change in the BTK L528W mutant is consistent
286 with the HDX-MS changes for this protein which suggest that the mutation has a slight stabilizing
287 effect on the compact autoinhibited conformation. Additionally, a new peak is observed as
288 expected in the BTK L528W mutant spectrum consistent with the introduction of an additional
289 tryptophan due to the mutation. Overall, as the BTK T474I and L528W mutations by themselves
290 cause only minor conformational changes, such changes are unlikely to constitute the mechanism
291 by which these mutations confer resistance.

292

293 *BTK L528W mutant activates the SRC family kinase HCK.*

294 Previous studies have shown that the BTK L528W mutant propagates BCR signaling
295 despite being catalytically dead [26, 43]. PLCγ phosphorylation and calcium signaling are
296 maintained in cells carrying this BTK mutation [26, 43]. This suggests that the BTK L528W
297 mutant might recruit other kinases to compensate for its lack of activity. The mechanism of action
298 of another catalytically inactive BTK resistant mutation: BTK C481F/Y, which arises in Ibrutinib
299 treated CLL patients, has been recently reported [44]. In that work the BTK C481F/Y resistance
300 mutant was shown to bind and activate the SRC family kinase HCK, thereby propagating signals

301 from the BCR signaling pathway [44]. This activation of HCK by BTK C481F/Y requires
302 phosphorylation on the BTK kinase activation loop, Y551. The phosphorylated Y551 is suggested
303 to bind to the HCK SH2 domain, displacing the autoinhibited conformation of HCK, thereby
304 activating the HCK catalytic function. To determine if a similar mechanism is at work for the
305 catalytically dead BTK L528W mutant, we tested the ability of the BTK L528W mutant to activate
306 HCK in a western blot assay by monitoring the phosphorylation levels on two substrates: PLCγ1
307 (pY783 phosphorylation) and HCK itself (pY levels). In addition, we also included BTK WT that
308 had been pre-incubated with Zanubrutinib as a control. As shown in Fig.7a,b, phosphorylation
309 increased on both PLCγ and HCK in the presence of full-length BTK L528W, suggesting that the
310 catalytically dead BTK mutant is able to activate HCK. Interestingly, Zanubrutinib bound WT
311 BTK also promoted increased phosphorylation levels on both PLCγ1 and HCK suggesting that
312 drug-inactivated BTK also activates HCK. This is distinct from what has been previously observed
313 for the BTK C481Y/F resistant mutation where, compared to WT BTK, the C481Y/F mutant BTK
314 preferentially engages HCK. Nevertheless, since the BTK L528W mutant activates HCK, we next
315 designed experiments to probe the requirements for this activation.

316 We first tested whether the regulatory domains of BTK were required for HCK activation
317 by the BTK L528W mutant by using the isolated linker kinase domain of BTK (a construct in
318 which the BTK regulatory domains have been deleted). As shown in Fig. 7c,d, the isolated linker
319 kinase domain of BTK L528W does not activate HCK. This suggests that the regulatory domain/s
320 of BTK are required for the activation of HCK and that the isolated linker kinase domain of BTK
321 alone is insufficient for HCK activation. This again is different from what has been previously
322 reported; the BTK C481Y/F resistant mutant requires the kinase domain for HCK activation [44].

323 We therefore turned our focus onto the BTK regulatory domains to isolate the specific region/s
324 required for HCK activation by the BTK L528W resistance mutation.

325 Displacement of the SH3 domain from its autoinhibitory conformation upon binding of a
326 proline-rich ligand is a classic mechanism by which SRC family kinases such as HCK are activated
327 [45]. BTK contains such a proline-rich ligand sequence within its regulatory region and so we
328 tested HCK activation by a BTK mutant lacking the proline-rich sequence (BTK L528W/Pro: BTK
329 L528W/ P189A/P192A/P203A/P206A). As shown in Fig. 7e,f, the BTK L528W proline-depleted
330 mutant does not activate HCK. This data again emphasizes the difference between the mechanism
331 of action of the BTK L528W mutant from the previously characterized BTK C481Y/F mutant.
332 Additionally, this data is consistent with the observation that WT BTK can also activate HCK, as
333 the proline-rich region is present in both WT and mutant L528W BTK. The ability of both WT
334 and L528W mutant BTK to activate HCK, however, suggests that there must be additional reasons
335 for the selection of the BTK L528W resistance mutation in patients.

336

337 *BTK L528W is more stable than WT BTK.*

338 Changes in protein levels have been shown to cause resistance in several cancers [46].
339 Cellular protein levels can be altered due to changes in protein expression, stability or degradation,
340 or changes at the RNA level [46]. An increase in BTK protein levels *in vivo* could drive protein-
341 protein interactions typically not observed in the WT background. Interestingly, we note that
342 protein yield after bacterial expression and purification of the full-length BTK L528W mutant is
343 higher than that of the WT protein, suggesting that the L528W mutant is more stable than the WT
344 protein. To test whether the BTK L528W mutation has a stabilizing effect on BTK, we measured

345 the melting temperature (Tm) of the BTK L528W mutant and compared it to that of the WT protein
346 in a thermal shift assay. As shown in Fig.7g, the BTK L528W mutant is more stable than the WT
347 protein (a one degree increase in Tm compared to the WT). The increased stability of the L528W
348 mutant, albeit small, could result in increased protein levels, an increase in the lifetime of the
349 protein or altered protein trafficking *in vivo*, all of which would drive the interaction of the mutant
350 protein with HCK unlike the WT protein.

351

352 *HDX-MS reveals that the BTK T474I and L528W mutants show reduced binding to BTK inhibitors.*

353 Disruption of inhibitor binding due to mutations is a classic mechanism by which resistance
354 arises [47, 48]. While loss of inhibitor binding is likely irrelevant to the catalytically dead BTK
355 L528W mutant, we nevertheless evaluated it along with the BTK T474I mutant using HDX-MS
356 and NMR. HDX-MS data show that Tirabrutinib, Zanubrutinib and Pirtobrutinib induce overall
357 changes in deuterium incorporation for both WT BTK and the T474I mutant (Fig. 8a,b,c) These
358 data suggest that the inhibitors are still capable of binding to the T474I mutant. However, in the
359 presence of Tirabrutinib, Zanubrutinib or Pirtobrutinib, the magnitude of the protection in the
360 kinase domain (N-lobe β2-β3 strands and activation loop) is consistently reduced in drug bound
361 T474I mutant as compared to the WT protein (Fig. 8a,b,c,e). The differences in deuterium
362 exchange for drug binding to WT and mutant BTK suggest that the T474I mutation either causes
363 a reduction in inhibitor binding or otherwise alters the mode of drug interaction in the active site.
364 Specifically, the peptides derived from the kinase activation loop in particular do not show as much
365 protection in the mutant relative to the WT suggesting that the inhibitors do not stabilize the
366 activation loop in the inactive conformation upon binding to the T474I mutant. Interestingly, the
367 changes observed in the BTK regulatory domains (SH3 and SH2 domains) upon Zanubrutinib,

368 Tirabrutinib or Pirtobrutinib binding to WT BTK as well as increased deuterium incorporation in
369 the G-helix of the kinase domain upon Tirabrutinib binding to WT BTK are maintained or reduced
370 slightly in the drug bound BTK T474I mutant. In stark contrast to the BTK T474I mutant, the BTK
371 L528W mutant does not show any change in deuterium incorporation in the presence of
372 Zanubrutinib, Tirabrutinib or Pirtobrutinib, providing strong evidence that the BTK L528W
373 mutant does not bind the inhibitors (Fig.8d). Taken together, both the BTK T474I and the BTK
374 L528W mutation impact inhibitor binding. Indeed, these results are consistent with previous
375 studies that show that the BTK T474I and the BTK L528W mutations disrupt binding to
376 Zanubrutinib and Pirtobrutinib [26]. We next tested the impact of the resistance mutations on
377 inhibitor binding by NMR.

378

379 *Probing the effects of BTK T474I and L528W mutations on inhibitor binding by NMR.*

380 Comparison of the Zanubrutinib bound WT BTK LKD spectrum to that of BTK T474I
381 shows that the BTK T474I mutant undergoes minor changes in the presence of Zanubrutinib,
382 suggesting that the mutant is binding weakly to the inhibitor (Fig. 9a, left and middle panels). The
383 W395 resonance shows little to no chemical shift change upon addition of Zanubrutinib to the
384 BTK T474I mutant, suggesting that this drug does not stabilize the inactive conformation of the
385 mutant kinase (Fig. 9a, middle panel). These results are consistent with HDX-MS changes in the
386 T474I mutant upon Zanubrutinib binding (Fig. 8a).

387 Spectral comparison of Tirabrutinib bound to WT and BTK T474I (Fig. 9b, left and middle
388 panels) shows drug induced chemical shift changes for both complexes, supporting the conclusion
389 from the HDX-MS data (Fig. 8b) that the drug binds to both WT and mutant BTK. However, the

390 spectral changes observed in the spectrum of Tirabrutinib bound to BTK T474I are different from
391 that of the WT/Tirabrutinib bound spectrum (Fig. 9b). Although BTK W395 gives rise to multiple
392 peaks in the spectra of Tirabrutinib bound to both WT and T474I, the W395 resonances in the
393 BTK T474I/Tirabrutinib complex are shifted upfield to a lesser extent compared to the same
394 resonance in the WT/Tirabrutinib spectrum. This suggests that the BTK T474I mutation alters the
395 binding to Tirabrutinib and the inactive kinase domain conformation (αC out) is less populated in
396 the drug bound mutant protein compared to WT BTK bound to Tirabrutinib. These results are
397 consistent with the HDX-MS results that show reduced protection in peptides corresponding to the
398 kinase activation loop in the mutant compared to WT due to the lack of stabilization of the kinase
399 inactive conformation upon Tirabrutinib binding.

400 Spectral overlay of the Pirtobrutinib bound BTK T474I with the apo T474I protein shows
401 pronounced chemical shift changes in the presence of the inhibitor, providing evidence consistent
402 with the HDX-MS data (Fig. 8c), that Pirtobrutinib binds the BTK T474I mutant (Fig. 9c, middle).
403 However, unlike Pirtobrutinib bound to WT BTK, multiple W395 peaks are visible in the spectrum
404 of Pirtobrutinib bound to BTK T474I. The resonance frequencies of the additional peaks are shifted
405 toward that of the apo protein suggesting the possibility of fast exchange between inhibitor bound
406 and unbound states. These observations suggest that the T474I mutation reduces affinity towards
407 Pirtobrutinib and are consistent with previously published SPR binding data [26].

408 BTK inhibitors that retain binding to the BTK T474I mutant could serve as potential
409 alternate treatment option for patients with this mutation. Additionally, the lack of or low
410 frequency of the BTK T474I mutation in patients treated with Ibrutinib and Acalabrutinib could
411 be due to the inability of this mutation to disrupt inhibitor binding. We therefore tested the ability
412 of the BTK T474I mutant to bind Ibrutinib, Acalabrutinib and Fenebrutinib (GDC-0853). The

413 NMR data suggest that the BTK T474I mutation does not impact Ibrutinib or Fenebrutinib binding
414 (Fig. 9d,f), but Acalabrutinib binding is reduced (Fig. 9e). Taken together, the T474I mutation
415 significantly reduces binding to Zanubrutinib, Tirabrutinib and Pirtobrutinib, retains binding to
416 Ibrutinib and Fenebrutinib, and may have an adverse effect on Acalabrutinib binding. Given that
417 the BTK T474I mutant retains activity (albeit reduced activity), disruption of drug binding is a
418 possible mechanism by which this mutation escapes inhibition.

419 Spectral overlays of the BTK L528W mutant with and without Zanubrutinib show no
420 chemical shift changes (Fig. 9a, right panel) suggesting that the mutation completely disrupts
421 inhibitor binding in complete agreement with the HDX-MS data (Fig. 8d). Tirabrutinib does show
422 chemical shift changes, but the changes are markedly different from that observed in the WT
423 protein (Fig. 9b, right). In the L528W spectrum in the presence of Tirabrutinib, W395 shifts in the
424 opposite downfield direction compared to the WT spectrum suggesting that Tirabrutinib could be
425 binding to the BTK L528W in a different orientation. Alternatively, the distinct chemical shift
426 change could be due to the mutated L528W residue altering the local chemical environment within
427 the kinase.

428 The Pirtobrutinib-bound BTK L528W spectrum (Fig. 9c) shows two resonance positions,
429 one of which overlaps with the W395 resonance in the apo protein and the other that corresponds
430 to that of the mutant protein bound to Pirtobrutinib. This data suggests a mixture of inhibitor bound
431 and unbound BTK kinase domain in solution, likely due to a reduction in Pirtobrutinib affinity
432 caused by the L528W mutation. Although the L528W mutation alters binding to both Tirabrutinib
433 and Pirtobrutinib, the NMR data suggests that it retains partial binding unlike the HDX-MS data
434 that suggests complete disruption of binding. The higher inhibitor concentrations used in the NMR
435 experiments compared to the HDX-MS experiments likely explain this discrepancy. Interestingly,

436 we note similarities between the BTK L528W Pirtobrutinib bound spectrum and that of
437 Tirabrutinib bound spectrum, suggesting that the BTK kinase domain adopts similar
438 conformations in solution when bound to these different drugs. Additionally, the BTK L528W
439 mutant retains binding to Fenebrutinib, however Ibrutinib and Acalabrutinib binding are disrupted
440 (Fig. 9d-f, right). Taken together, the BTK L528W mutation significantly disrupts Zanubrutinib,
441 Tirabrutinib and Pirtobrutinib binding. However, drugs based on Fenebrutinib could be developed
442 to treat patients carrying this mutation (see discussion below).

443

444 DISCUSSION

445 Binding of BTK active site inhibitors can have long-range effects on the protein. Here, we
446 build on earlier work to show that three of the clinically approved BTKi (Acalabrutinib,
447 Zanubrutinib and Tirabrutinib) shift the conformational ensemble of full-length BTK,
448 destabilizing the autoinhibited conformation of the SH3 and SH2 domains to varying degrees
449 (Fig.4 and 5). In marked contrast, Pirtobrutinib led to the stabilization of the compact autoinhibited
450 conformation of full-length BTK. The exposure or stabilization of the regulatory domains of BTK
451 by active site BTK inhibitors can alter the interaction of BTK with ligands *in vivo*. Indeed, BTK
452 inhibitors have been shown to differ in their effectiveness at terminating signals downstream of
453 the Fc receptor *versus* the B cell receptor [49, 50]. As more BTKi become available, a molecular-
454 level understanding of the interaction of the inhibitor with full-length BTK will aid the
455 interpretation of the efficacy of different BTK inhibitors in treating disease states driven by
456 different signaling pathways.

457 The development of specific resistance mutations in patients treated with different BTKi is
458 intriguing. Covalent BTKi rely on BTK C481 within the kinase active site. The C481S mutation
459 prevents the covalent attachment of these inhibitors to BTK and converts the mode of binding of
460 these drugs to that of a reversible inhibitor. Importantly, we and others have shown that the BTK
461 C481S mutation does not prevent binding of Ibrutinib to the BTK kinase domain [16, 26]. In fact,
462 the BTK C481S mutant binds to Ibrutinib just as well as the WT protein *in vitro* under equilibrium
463 conditions where drug concentrations do not vary over time [16]. However, *in vivo*, drug
464 concentrations change with time; inhibitor concentrations peak rapidly after intake followed by a
465 decrease as the drug is cleared (represented by the half-life of the drug). The occupancy of BTK
466 C481S protein by these covalent inhibitors in patients is therefore dictated by the availability of

467 these covalent inhibitors over time. Interestingly, Ibrutinib and Acalabrutinib have short half-lives
468 compared to Zanubrutinib and Tirabrutinib (Table 1). The short half-lives of Ibrutinib and
469 Acalabrutinib suggests that the BTK C481S mutant is likely to be unoccupied when inhibitor
470 concentrations fall, thereby allowing the BTK C481S mutant to escape from inhibition.
471 Conversely, the longer half-life of Zanubrutinib and Tirabrutinib in patients suggests that the BTK
472 C481S mutant is likely to remain occupied (inhibited) for a longer period of time. The C481S
473 mutation therefore does not offer a selective advantage as a resistance mutation in Zanubrutinib
474 and Tirabrutinib treated patients and likely explains the lower frequency of occurrence of this
475 mutation in these patients compared to Ibrutinib and Acalabrutinib treated patients. Taken
476 together, the BTK C481S mutant can escape covalent inhibition at low drug concentrations *in vivo*
477 and is therefore predicted to arise in patients treated with BTK covalent inhibitors that have short
478 half-lives.

479 The T474I mutation arises frequently in Tirabrutinib and Pirtobrutinib treated CLL patients
480 (Fig. 1d). Our HDX-MS and NMR binding studies show that the T474I mutation disrupts binding
481 to both inhibitors. Reduced binding of BTK T474I mutant to Tirabrutinib and Pirtobrutinib, along
482 with the partial catalytic activity retained by this mutant, would allow BTK T474I mutant to escape
483 inhibition and maintain BCR signaling. This gives a selective advantage to the cells that carry this
484 mutation. Additionally, our NMR binding studies show that the BTK T474I mutation does not
485 disrupt binding of Ibrutinib. This is consistent with the low occurrence of this mutation in
486 Ibrutinib-treated CLL patients. While the BTK T474I mutation does seem to disrupt binding to
487 Acalabrutinib, the lower activity of the T474I mutant (compared to the BTK C481S mutant) may
488 explain the higher prevalence of the BTK C481S mutation (compared to T474I) in Acalabrutinib
489 treated patients.

490

491 *Ideas and Speculation*

492 Successful treatment of CLL has relied on the inhibition of BTK catalytic activity to curb
493 BCR signaling. Inhibitor-bound, catalytically-inactive BTK is incapable of propagating BCR
494 signaling. Paradoxically, the catalytically inactive BTK L528W mutant is able to propagate BCR
495 signals [26, 43]. A similar catalytically inactive BTK mutant, the BTK C481Y/F resistance
496 mutation also arises in Ibrutinib and Acalabrutinib treated patients, albeit at a low frequency [44].
497 Since these BTK mutants are catalytically dead, other kinases must compensate for the absence of
498 BTK activity to account for the intact BCR signaling in these patients. Exogenous kinases do not
499 appear to compensate for WT BTK that is inactivated by BTK inhibitors, and so there must be
500 additional differences between the catalytically dead (BTK L528W and BTK C481Y/F) mutant
501 kinases and inhibitor bound WT BTK that is rendered catalytically inactive by virtue of drug
502 binding. Our HDX-MS and NMR data show that BTK L528W mutation does not drastically
503 change the conformation of BTK. However, this mutation does increase the stability of BTK
504 compared to the WT protein. This increased stability could alter protein levels or change the
505 trafficking/localization of the mutant protein *in vivo* which in turn could alter protein-protein
506 interactions that drive activation of an alternate kinase such as HCK *in vivo*. Comparison of BTK
507 protein levels in patients pre- and post-development of resistance will be needed to test this
508 hypothesis. Alternatively, the BTK L528W mutation may require an additional change/s in the cell
509 that allow for this dead kinase to recruit other kinases such as HCK to propagate BCR signaling.
510 This requirement for additional changes may explain the low frequency of the L528W mutation in
511 Ibrutinib and Acalabrutinib treated patients; the single amino acid change, C481S, combined with
512 the rapid clearance of drug seems sufficient to drive resistance. Finally, the absence of the BTK

513 L528W resistance mutation in Ibrutinib treated CLL patients could be due to the promiscuity of
514 Ibrutinib; candidate compensatory kinases may be inactivated by the drug [51]. The increased
515 specificity of Zanubrutinib, Tirabrutinib and Pirtobrutinib on the other hand could allow for the
516 utilization of compensatory kinases such as HCK by BTK L528W in order to propagate BCR
517 signaling.

518 Understanding the mechanism/s by which resistance mutations evade inhibition allows for
519 counter strategies to be devised [52-54]. The reversible BTK inhibitor Pirtobrutinib is able to
520 inhibit the BTK C481S mutant due to its long serum half-life and has been suggested as a treatment
521 option for patients that develop this mutation [55]. Alternatively, drug occupancy in the context of
522 the BTK C481S resistance mutant could be increased by administering a twice daily dose of the
523 inhibitor as opposed to the single daily dose possibly circumventing their short half-lives [56].
524 This increased exposure time to the covalent inhibitor could cause increased side effects and so
525 such risks should be considered before altering the dosage regimen. Alternatively, Tirabrutinib,
526 which exhibits the longest half-life among the available covalent BTK inhibitors, could be used to
527 slow progression of disease in patients that develop the C481S resistance mutation.

528 The BTK T474I mutation disrupts binding to Zanubrutinib, Tirabrutinib, Pirtobrutinib and
529 Acalabrutinib (Fig.8, 9) but retains binding to Ibrutinib and Fenebrutinib creating possible options
530 for patients that develop the BTK T474I resistance mutation. The BTK L528W mutant is
531 catalytically inactive, hence treatment with any BTK active site inhibitor is futile. Previous studies
532 have shown that the similarly inactive BTK C481Y/F mutant can be suppressed by the use of
533 PROTACS to induce degradation of the full-length protein [44]. Importantly, our data indicate that
534 although the BTK L528W mutation disrupted binding to most BTK inhibitors it retains binding to
535 Fenebrutinib (Fig.9), suggesting that PROTACS based on Fenebrutinib or similar backbones could

536 be developed to treat this resistance mutation [57]. Alternate treatment approaches such as
537 targeting HCK or other BCR signaling proteins such as BCL-2 [58] could also be used to counter
538 this resistance mutation. As additional patient data becomes available, the patterns of resistance
539 mutations for different inhibitors will become clearer and strategies to circumvent resistance using
540 existing inhibitors should improve. As for many areas of medicine, the treatment landscape should
541 benefit from the ongoing era of personalized medicine.

542

543 MATERIALS AND METHODS

544 *Constructs and reagents*: The bacterial expression constructs for murine BTK linker kinase
545 domain (LKD) and full-length (FL) have been described previously [39]. All BTK constructs carry
546 the solubilizing Y617P mutation for bacterial expression [39]. All mutations were made using the
547 site directed mutagenesis kit (Agilent), and the sequences of all constructs were confirmed by
548 sequencing at the Iowa State University DNA facility. Acalabrutinib, Zanubrutinib, Tirabrutinib
549 and Pirtobrutinib were purchased from MedChem Express. Ibrutinib was purchased from
550 Selleckchem. The pCDF-1 Duet HCK SH3-SH2-Kinase domain/YopH construct with a 'YEEI'
551 tail, a kind gift from Dr. Tom Smithgall, was mutated to convert the 'YEEI' tail residues to that of
552 the WT protein (YQQQ). The pGEX PLCγ1 cSH2-linker Y771F/Y775F protein substrate
553 construct has been described previously [59].

554

555 *Protein expression and purification*: Expression and purification of the PLCγ1 cSH2-linker
556 Y771F/Y775F protein substrate has been described previously [59]. HCK, Full-length BTK and
557 BTK linker kinase domain (WT and mutants) were produced by co-expressing with YopH in

558 BL21(DE3) (Millipore Sigma) or BL21-Gold(DE3) cells (Agilent Technologies) as described
559 previously [39]. Briefly, the culture was grown at 37 °C to an O.D. 600 nm of 0.6 to 0.8. The
560 temperature of the culture was lowered to 18°C and then induced with either 1.0 mM IPTG for
561 BTK LKD construct or 0.1 mM IPTG for BTK full-length and HCK. The culture was harvested
562 24 hours after induction and the pellets were resuspended in lysis buffer (50 mM KH_2PO_4, pH 8.0,
563 150 mM NaCl, 20 mM imidazole and 0.5 mg/ml lysozyme) and stored at -80°C. Cells were lysed
564 by thawing and the action of lysozyme, and 3000 U DNAse I (Sigma) and 1 mM PMSF were
565 added to the lysate, incubated at RT for 20 minutes and then spun at 16,000 rpm for one hour at
566 4°C. Glycerol was added to the supernatant to a final concentration of 10 % and was then incubated
567 with Ni-NTA resin (QIAGEN) for two hours, washed with Tris pH 8.0, 75 mM NaCl, 40 mM
568 imidazole, and eluted in 20 mM Tris pH 8.0, 150 mM NaCl, 250 mM Imidazole, and 10% glycerol.
569 Eluted protein was flash frozen in liquid nitrogen and stored at -80°C. The proteins were
570 concentrated and further purified by size exclusion chromatography (Hiload Superdex 26/60 200
571 pg or Hiload Superdex 26/60 75 pg, GE Healthcare). The fractions containing pure protein were
572 pooled, concentrated, snap frozen and stored at -80° C. The final buffer consists of 20 mM Tris
573 pH 8.0, 150 mM Sodium chloride, 0.02 % Sodium azide and 10% glycerol. Initial phosphorylation
574 levels of all purified BTK and HCK proteins used in this study is below western immuno-detection.

575

576 *NMR*: Uniformly ^{15}N labeled BTK samples were produced as described earlier by growth in
577 modified M9 minimal media containing ^{15}N ammonium chloride (1g/L, Cambridge Isotope
578 Laboratories, Inc.) as the sole source of nitrogen [39]. The final NMR sample buffer consists of
579 20 mM Tris, 150 mM Sodium chloride, 10% glycerol, and 0.02 % Sodium azide at pH 8.0. All
580 NMR spectra were collected at 298 K on a Bruker AVIII HD 800 spectrometer equipped with a 5

581 mm HCN z-gradient cryoprobe operating at a ^{1}H frequency of 800.37 NMR samples with
582 inhibitors consisted of 150 μM ^{15}N labeled BTK, mixed with 200 μM inhibitor in 2% DMSO. All
583 data were analyzed using NMRViewJ [60].

584

585 *HDX-MS:* General procedures for HDX-MS of BTK have been described in detail previously [39].
586 Details specific to experiments conducted here are provided in the Supplemental Datafile in the
587 format recommended [61] for HDX-MS experimental descriptions. All HDX-MS data have been
588 deposited to the ProteomeXchange Consortium via the PRIDE [62] partner repository with the
589 dataset identifier PXD047865. Briefly, prior to continuous labeling HDX experiments, purified
590 BTK full-length wild-type, T474I or L528W (20 μM) and inhibitor (40 μM), (20 mM Tris pH 8.0,
591 150mM NaCl, 10% glycerol, 2% DMSO) were allowed to interact at 21 °C for 1 hour. After the
592 binding reactions, both the free kinase and kinase bound to inhibitor were placed on ice prior to
593 deuterium labeling. Deuterium labeling proceeded for the times described using labeling buffer,
594 and labeling was stopped with an equal volume of quench buffer at 0°C (details in Supplemental
595 Datafile). Quenched samples were immediately analyzed using a Waters nanoACQUITY with
596 HDX technology using online pepsin digestion with a Waters Enzymate immobilized pepsin
597 column and UPLC separation of the resulting peptic peptides. Mass spectra were acquired using a
598 Waters Synapt $HDMS^{E}$ mass spectrometer. Peptides generated from online pepsin digestion were
599 identified with Waters Protein Lynx Global Server 3.0 using separate unlabeled protein that was
600 prepared in the same manner as protein labeled with deuterium. Deuterium incorporation was
601 quantified using Waters DynamX 3.0. Deuterium levels for each peptide were calculated by
602 subtracting the average mass of the undeuterated control sample from that of the deuterium labeled
603 sample; the data were not corrected for back exchange and are therefore reported as relative [63].

604 Vertical difference maps in Figures 4, 6 and 8 do not represent a linear sequence of non-
605 overlapping peptides. All coincident and overlapping peptides for comparisons in each figure are
606 provided in figure identified tabs of the Supplemental Datafile.

607

608 *Activity assays*: *In vitro* kinase assays were performed as described previously [39]. Briefly, 1 μM
609 BTK FL, BTK FL T474I or BTK FL L528W proteins were incubated in a kinase assay buffer (50
610 mM Hepes pH 7.0, 10 mM $MgCl_2$, 1 mM DTT, 5 % glycerol, 1 mM Pefabloc, and 200 μM ATP)
611 at room temperature for varying time. The reactions were stopped by the addition of SDS-PAGE
612 loading buffer and the samples were boiled, separated by SDS−PAGE, and Western blotted with
613 the anti-BTK pY551 antibody (BD Pharmingen™) or anti-His antibody (EMD Millipore) as
614 described previously [39]. The bands were quantified using the ChemiDoc™ (Biorad) gel imaging
615 system. The phosphorylation levels (Anti-BTK pY551 blot) were normalized to the total protein
616 level (Anti-His blot). The BTK FL value at 40 minutes was set to 1 and compared to BTK FL
617 T474I or BTK FL L528W. The HCK activation experiments were performed by preincubating 0.2
618 μM of BTK WT or L528W proteins with 0.5 μM Zanubrutinib for 15 min at RT. The reaction was
619 initiated with the addition of 0.2 μM HCK in a kinase assay buffer (50 mM Hepes pH 7.0, 10 mM
620 $MgCl_2$, 1 mM DTT, 5 % glycerol, 1 mM Pefabloc, 30 μM PLCγ1 cSH2 linker Y771F/Y775F
621 substrate and 200 μM ATP). Time points were taken at 5, 10 and 15 minutes. The reactions were
622 stopped by the addition of SDS-PAGE loading buffer and the samples were boiled, separated by
623 SDS−PAGE, and Western blotted with the anti-PLCγ1-pY783 antibody (Cell Signaling) or anti-
624 pY antibody (4G10, Millipore Sigma) or anti-His antibody (EMD Millipore) as described
625 previously [39]. The bands were quantified using the ChemiDoc™ (Biorad) gel imaging system.
626 The HCK alone value was set to 1 and compared to HCK + BTK WT/L528W. Initial

627 phosphorylation levels of BTK, prior to the start of the activity assay were undetectable by western
628 immuno-detection.

629

630 *Thermal shift assays*: BTK FL WT or mutant at 5 μM was incubated with 10X final concentration
631 of SYPRO Orange dye (Thermo Fisher Scientific) in a total volume of 20 μL Tris buffer (20 mM
632 Tris, 150 mM Sodium chloride, 10% glycerol, pH 8.0). Thermal shift assays were performed on
633 the StepOnePlus RT-PCR machine in the Iowa State University DNA Facility. The temperature
634 was raised from 25 °C to 95 °C and measurements recorded with every 0.5 °C increment in
635 temperature. The derivative plot of the data was analyzed for the melting temperature (Tm). Assays
636 were performed thrice and the average Tm was calculated.

637

638 ACKNOWLEDGEMENTS

639 This work is supported by a grant from the National Institutes of Health (National Institute
640 of Allergy and Infectious Diseases, AI43957) to A.H.A., J.R.E and T.E.W., and by funds from the
641 Scott-Waudby Trust, the Hope Against Cancer charity, Cancer Research UK in conjunction with
642 the UK Department of Health on an Experimental Cancer Medicine Centre grant
643 [C10604/A25151] to S.J, R.G.B and M.J.SD. Research at the University of Leicester was carried
644 out at the National Institute for Health and Care Research (NIHR) Leicester Biomedical Research
645 Centre (BRC). The authors also thank the Roy J. Carver Charitable Trust, Muscatine, Iowa for
646 ongoing research support.

647

648 REFERENCES

649 1. Burger, J.A., et al., *Ibrutinib as Initial Therapy for Patients with Chronic Lymphocytic Leukemia.* N
650 Engl J Med, 2015. **373**(25): p. 2425-37.
651 2. Davids, M.S. and J.R. Brown, *Ibrutinib: a first in class covalent inhibitor of Bruton's tyrosine kinase.*
652 Future Oncol, 2014. **10**(6): p. 957-67.
653 3. Honigberg, L.A., et al., *The Bruton tyrosine kinase inhibitor PCI-32765 blocks B-cell activation and*
654 *is efficacious in models of autoimmune disease and B-cell malignancy.* Proc Natl Acad Sci U S A,
655 2010. **107**(29): p. 13075-80.
656 4. Herman, S.E., et al., *Bruton tyrosine kinase represents a promising therapeutic target for*
657 *treatment of chronic lymphocytic leukemia and is effectively targeted by PCI-32765.* Blood, 2011.
658 **117**(23): p. 6287-96.
659 5. Rozkiewicz, D., et al., *Bruton's Tyrosine Kinase Inhibitors (BTKIs): Review of Preclinical Studies and*
660 *Evaluation of Clinical Trials.* Molecules, 2023. **28**(5).
661 6. Shirley, M., *Bruton Tyrosine Kinase Inhibitors in B-Cell Malignancies: Their Use and Differential*
662 *Features.* Target Oncol, 2022. **17**(1): p. 69-84.
663 7. Montoya, S. and M.C. Thompson, *Non-Covalent Bruton's Tyrosine Kinase Inhibitors in the*
664 *Treatment of Chronic Lymphocytic Leukemia.* Cancers (Basel), 2023. **15**(14).
665 8. Kueffer, L.E., R.E. Joseph, and A.H. Andreotti, *Reining in BTK: Interdomain Interactions and Their*
666 *Importance in the Regulatory Control of BTK.* Front Cell Dev Biol, 2021. **9**: p. 655489.
667 9. Frustaci, A.M., et al., *Next Generation BTK Inhibitors in CLL: Evolving Challenges and New*
668 *Opportunities.* Cancers (Basel), 2023. **15**(5).
669 10. Mendes-Bastos, P., et al., *Bruton's tyrosine kinase inhibition-An emerging therapeutic strategy in*
670 *immune-mediated dermatological conditions.* Allergy, 2022. **77**(8): p. 2355-2366.
671 11. Robak, E. and T. Robak, *Bruton's Kinase Inhibitors for the Treatment of Immunological Diseases:*
672 *Current Status and Perspectives.* J Clin Med, 2022. **11**(10).
673 12. Byrd, J.C., et al., *Acalabrutinib Versus Ibrutinib in Previously Treated Chronic Lymphocytic*
674 *Leukemia: Results of the First Randomized Phase III Trial.* J Clin Oncol, 2021. **39**(31): p. 3441-3452.
675 13. Brown, J.R., et al., *Zanubrutinib or Ibrutinib in Relapsed or Refractory Chronic Lymphocytic*
676 *Leukemia.* N Engl J Med, 2023. **388**(4): p. 319-332.
677 14. Lovell, A.R., N. Jammal, and P. Bose, *Selecting the optimal BTK inhibitor therapy in CLL: rationale*
678 *and practical considerations.* Ther Adv Hematol, 2022. **13**: p. 20406207221116577.
679 15. Buske, C., et al., *Managing Waldenstrom's macroglobulinemia with BTK inhibitors.* Leukemia,
680 2023. **37**(1): p. 35-46.
681 16. Joseph, R.E., et al., *Differential impact of BTK active site inhibitors on the conformational state of*
682 *full-length BTK.* Elife, 2020. **9**.
683 17. Sonti, R., et al., *ATP Site Ligands Determine the Assembly State of the Abelson Kinase Regulatory*
684 *Core via the Activation Loop Conformation.* J Am Chem Soc, 2018. **140**(5): p. 1863-1869.
685 18. Tong, M., et al., *Survey of solution dynamics in Src kinase reveals allosteric cross talk between the*
686 *ligand binding and regulatory sites.* Nat Commun, 2017. **8**(1): p. 2160.
687 19. Skora, L., et al., *NMR reveals the allosteric opening and closing of Abelson tyrosine kinase by ATP-*
688 *site and myristoyl pocket inhibitors.* Proc Natl Acad Sci U S A, 2013. **110**(47): p. E4437-45.
689 20. Sedlarikova, L., et al., *Resistance-Associated Mutations in Chronic Lymphocytic Leukemia Patients*
690 *Treated With Novel Agents.* Front Oncol, 2020. **10**: p. 894.
691 21. Maddocks, K.J., et al., *Etiology of Ibrutinib Therapy Discontinuation and Outcomes in Patients With*
692 *Chronic Lymphocytic Leukemia.* JAMA Oncol, 2015. **1**(1): p. 80-7.

693 22. Ahn, I.E., et al., *Clonal evolution leading to ibrutinib resistance in chronic lymphocytic leukemia.*
694 Blood, 2017. **129**(11): p. 1469-1479.
695 23. Woyach, J.A., et al., *Resistance mechanisms for the Bruton's tyrosine kinase inhibitor ibrutinib.* N
696 Engl J Med, 2014. **370**(24): p. 2286-94.
697 24. Blombery, P., et al., *Enrichment of BTK Leu528Trp mutations in patients with CLL on zanubrutinib:*
698 *potential for pirtobrutinib cross-resistance.* Blood Adv, 2022. **6**(20): p. 5589-5592.
699 25. Furman, R.R., et al., *Ibrutinib resistance in chronic lymphocytic leukemia.* N Engl J Med, 2014.
700 **370**(24): p. 2352-4.
701 26. Wang, E., et al., *Mechanisms of Resistance to Noncovalent Bruton's Tyrosine Kinase Inhibitors.* N
702 Engl J Med, 2022. **386**(8): p. 735-743.
703 27. Jackson, R.A., et al., *BTK mutations in patients with chronic lymphocytic leukemia receiving*
704 *tirabrutinib.* Blood Adv, 2023. **7**(14): p. 3378-3381.
705 28. Handunnetti SM, T.C., Nguyen T, et al., *BTK Leu528Trp - a Potential Secondary Resistance*
706 *Mechanism Specific for Patients with Chronic Lymphocytic Leukemia Treated with the Next*
707 *Generation BTK Inhibitor Zanubrutinib.* Blood., 2019. **134**: p. 170.
708 29. Woyach, J.A., Huang, Y., Rogers, K., Bhat, S.A., et al., *Resistance to Acalabrutinib in CLL Is Mediated*
709 *Primarily By BTK Mutations.* Blood, 2019. **134**: p. 504.
710 30. Woyach, J.A., et al., *BTK(C481S)-Mediated Resistance to Ibrutinib in Chronic Lymphocytic*
711 *Leukemia.* J Clin Oncol, 2017. **35**(13): p. 1437-1443.
712 31. Nakhoda, S., A. Vistarop, and Y.L. Wang, *Resistance to Bruton tyrosine kinase inhibition in chronic*
713 *lymphocytic leukaemia and non-Hodgkin lymphoma.* Br J Haematol, 2023. **200**(2): p. 137-149.
714 32. Kanagal-Shamanna, R., et al., *Targeted multigene deep sequencing of Bruton tyrosine kinase*
715 *inhibitor-resistant chronic lymphocytic leukemia with disease progression and Richter*
716 *transformation.* Cancer, 2019. **125**(4): p. 559-574.
717 33. Gango, A., et al., *Dissection of subclonal evolution by temporal mutation profiling in chronic*
718 *lymphocytic leukemia patients treated with ibrutinib.* Int J Cancer, 2020. **146**(1): p. 85-93.
719 34. Sharma, S., et al., *Identification of a structurally novel BTK mutation that drives ibrutinib resistance*
720 *in CLL.* Oncotarget, 2016. **7**(42): p. 68833-68841.
721 35. Xie, Q., et al., *Substrate recognition of PLCgamma1 via a specific docking surface on Itk.* J Mol Biol,
722 2013. **425**(4): p. 683-96.
723 36. Lin, D.Y. and A.H. Andreotti, *Structure of BTK kinase domain with the second-generation inhibitors*
724 *acalabrutinib and tirabrutinib.* PLoS One, 2023. **18**(8): p. e0290872.
725 37. Gomez, E.B., et al., *Preclinical characterization of pirtobrutinib, a highly selective, noncovalent*
726 *(reversible) BTK inhibitor.* Blood, 2023. **142**(1): p. 62-72.
727 38. Guo, Y., et al., *Discovery of Zanubrutinib (BGB-3111), a Novel, Potent, and Selective Covalent*
728 *Inhibitor of Bruton's Tyrosine Kinase.* J Med Chem, 2019. **62**(17): p. 7923-7940.
729 39. Joseph, R.E., et al., *Achieving a Graded Immune Response: BTK Adopts a Range of Active/Inactive*
730 *Conformations Dictated by Multiple Interdomain Contacts.* Structure, 2017. **25**(10): p. 1481-1494
731 e4.
732 40. Lin, D.Y., Kueffer, L.E., Juneja, P., Wales, T., et al., *Conformational heterogeneity of the BTK PHTH*
733 *domain drives multiple regulatory states.* eLife, 2023.
734 41. Wang, Q., et al., *Autoinhibition of Bruton's tyrosine kinase (Btk) and activation by soluble inositol*
735 *hexakisphosphate.* Elife, 2015. **4**.
736 42. Johnson, A.R., et al., *Battling Btk Mutants With Noncovalent Inhibitors That Overcome Cys481 and*
737 *Thr474 Mutations.* ACS Chem Biol, 2016. **11**(10): p. 2897-2907.
738 43. Yuan, H., et al., *BTK kinase activity is dispensable for the survival of diffuse large B-cell lymphoma.*
739 J Biol Chem, 2022. **298**(11): p. 102555.

740 44. Dhami, K., et al., *Kinase-deficient BTK mutants confer ibrutinib resistance through activation of the*
741 *kinase HCK.* Sci Signal, 2022. **15**(736): p. eabg5216.
742 45. Moarefi, I., et al., *Activation of the Src-family tyrosine kinase Hck by SH3 domain displacement.*
743 Nature, 1997. **385**(6617): p. 650-3.
744 46. Pessoa, J., et al., *Editorial: Altered Expression of Proteins in Cancer: Function and Potential*
745 *Therapeutic Targets.* Front Oncol, 2022. **12**: p. 949139.
746 47. Bhullar, K.S., et al., *Kinase-targeted cancer therapies: progress, challenges and future directions.*
747 Mol Cancer, 2018. **17**(1): p. 48.
748 48. Cohen, P., D. Cross, and P.A. Janne, *Kinase drug discovery 20 years after imatinib: progress and*
749 *future directions.* Nat Rev Drug Discov, 2021. **20**(7): p. 551-569.
750 49. Bender, A.T., et al., *Ability of Bruton's Tyrosine Kinase Inhibitors to Sequester Y551 and Prevent*
751 *Phosphorylation Determines Potency for Inhibition of Fc Receptor but not B-Cell Receptor*
752 *Signaling.* Mol Pharmacol, 2017. **91**(3): p. 208-219.
753 50. Li, W., et al., *Bruton's Tyrosine Kinase Inhibitors With Distinct Binding Modes Reveal Differential*
754 *Functional Impact on B-Cell Receptor Signaling.* Mol Cancer Ther, 2023.
755 51. Yang, G., et al., *HCK is a survival determinant transactivated by mutated MYD88, and a direct*
756 *target of ibrutinib.* Blood, 2016. **127**(25): p. 3237-52.
757 52. Skanland, S.S. and A.R. Mato, *Overcoming resistance to targeted therapies in chronic lymphocytic*
758 *leukemia.* Blood Adv, 2021. **5**(1): p. 334-343.
759 53. Smith, C.I.E. and J.A. Burger, *Resistance Mutations to BTK Inhibitors Originate From the NF-kappaB*
760 *but Not From the PI3K-RAS-MAPK Arm of the B Cell Receptor Signaling Pathway.* Front Immunol,
761 2021. **12**: p. 689472.
762 54. Alexandra Chirino, S.M., Anita Safronenka and Justin Taylor, *Resisting the Resistance: Navigating*
763 *BTK Mutations in Chronic Lymphocytic Leukemia (CLL).* Genes, 2023. **14**: p. 2182.
764 55. Aslan, B., et al., *Pirtobrutinib inhibits wild-type and mutant Bruton's tyrosine kinase-mediated*
765 *signaling in chronic lymphocytic leukemia.* Blood Cancer J, 2022. **12**(5): p. 80.
766 56. Skanland, S.S. and G.E. Tjonnfjord, *Determining drug dose in the era of targeted therapies: playing*
767 *it (un)safe?* Blood Cancer J, 2022. **12**(8): p. 123.
768 57. Zorba, A., et al., *Delineating the role of cooperativity in the design of potent PROTACs for BTK.* Proc
769 Natl Acad Sci U S A, 2018. **115**(31): p. E7285-E7292.
770 58. Molica, S., *Venetoclax: a real game changer in treatment of chronic lymphocytic leukemia.* Int J
771 Hematol Oncol, 2020. **9**(4): p. IJH31.
772 59. Joseph, R.E., et al., *A remote substrate docking mechanism for the tec family tyrosine kinases.*
773 Biochemistry, 2007. **46**(18): p. 5595-603.
774 60. Johnson, B.A. and R.A. Blevins, *NMR View: A computer program for the visualization and analysis*
775 *of NMR data.* J Biomol NMR, 1994. **4**(5): p. 603-14.
776 61. Masson, G.R., et al., *Recommendations for performing, interpreting and reporting hydrogen*
777 *deuterium exchange mass spectrometry (HDX-MS) experiments.* Nat Methods, 2019. **16**(7): p. 595-
778 602.
779 62. Vizcaino, J.A., et al., *2016 update of the PRIDE database and its related tools.* Nucleic Acids Res,
780 2016. **44**(22): p. 11033.
781 63. Wales, T.E. and J.R. Engen, *Hydrogen exchange mass spectrometry for the analysis of protein*
782 *dynamics.* Mass Spectrom Rev, 2006. **25**(1): p. 158-70.
783 64. Advani, R.H., et al., *Bruton tyrosine kinase inhibitor ibrutinib (PCI-32765) has significant activity in*
784 *patients with relapsed/refractory B-cell malignancies.* J Clin Oncol, 2013. **31**(1): p. 88-94.
785 65. Podoll, T., et al., *Bioavailability, Biotransformation, and Excretion of the Covalent Bruton Tyrosine*
786 *Kinase Inhibitor Acalabrutinib in Rats, Dogs, and Humans.* Drug Metab Dispos, 2019. **47**(2): p. 145-
787 154.

788 66. Tam, C.S., et al., *Phase 1 study of the selective BTK inhibitor zanubrutinib in B-cell malignancies*
789 *and safety and efficacy evaluation in CLL.* Blood, 2019. **134**(11): p. 851-859.
790 67. Walter, H.S., et al., *A phase 1 clinical trial of the selective BTK inhibitor ONO/GS-4059 in relapsed*
791 *and refractory mature B-cell malignancies.* Blood, 2016. **127**(4): p. 411-9.
792 68. Mato, A.R., et al., *Pirtobrutinib in relapsed or refractory B-cell malignancies (BRUIN): a phase 1/2*
793 *study.* Lancet, 2021. **397**(10277): p. 892-901.

794

795

FIGURES

Figure 1:

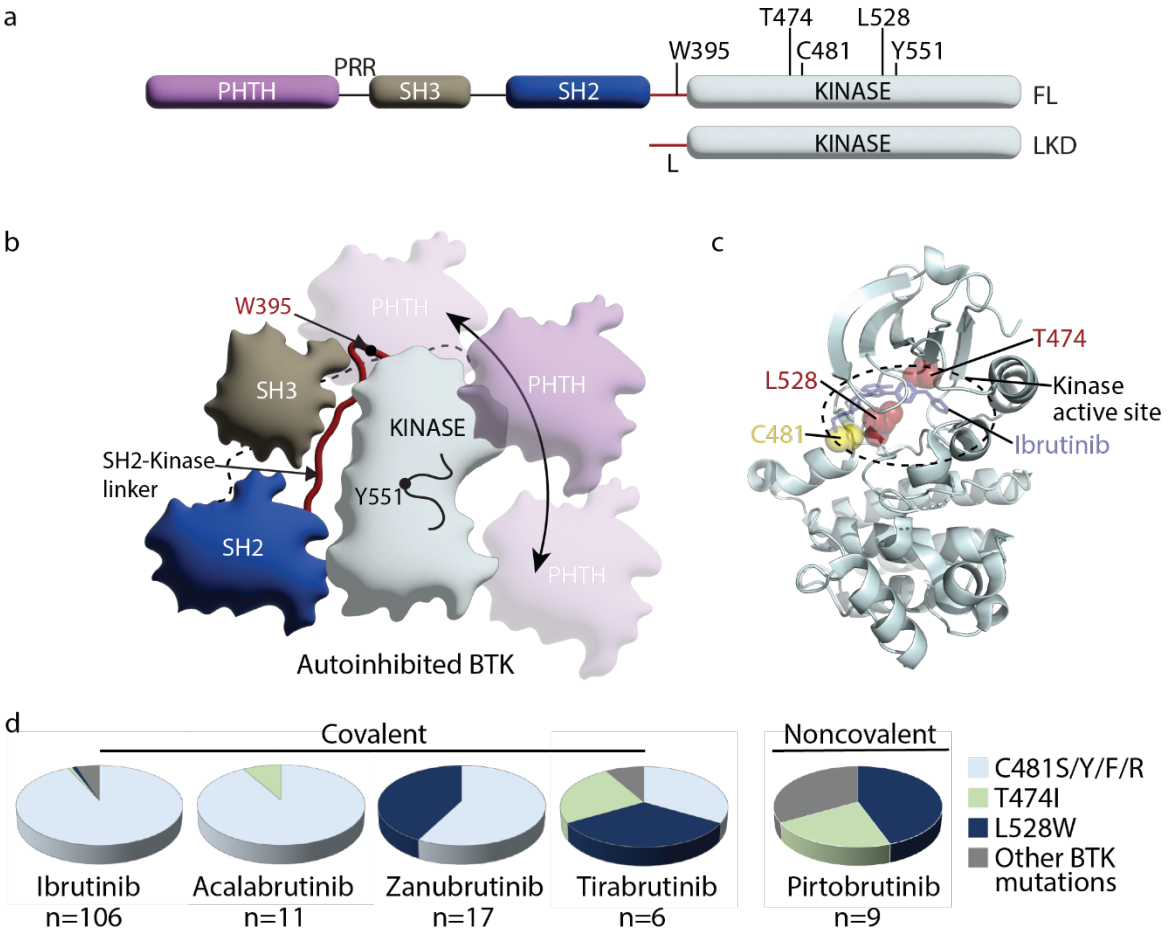

Figure 1: (a) Domain organization of full-length (FL) BTK and the BTK linker-kinase domain (LKD) fragment used in this study: PHTH, Pleckstrin homology-Tec homology domain; PRR, proline-rich region; SH3, Src homology 3 domain; SH2, Src homology 2 domain, SH2-kinase linker (L) and the catalytic kinase domain. Key residues are indicated above each domain. (b) Autoinhibited conformation of FL BTK based on the crystal structure of FL BTK [40]. The PHTH domain (purple) is dynamic, in transient contact with several regions on the core SH3-SH2-kinase

806 domain and is not visible in the crystal structure of full-length BTK [40]. Dynamics of the PHTH
807 domain is represented by the multiple poses of the PHTH domain and the double headed arrow.
808 (c) Co-crystal structure of BTK LKD (light cyan cartoon) bound to Ibrutinib (PDB ID: 5P9J)
809 showing the location of C481 (yellow spheres), T474 and L528 (red spheres) within the kinase
810 active site (broken oval). (c) Pie charts showing the prevalence of the BTK resistance mutations
811 in CLL patients treated with various BTK inhibitors. The total number of patients with mutations
812 in BTK are indicated below each chart. See Supp. Table 1 for additional details.

813

814

815

816

817

818

819

820

821

822

823

824

825

826 Figure 2:

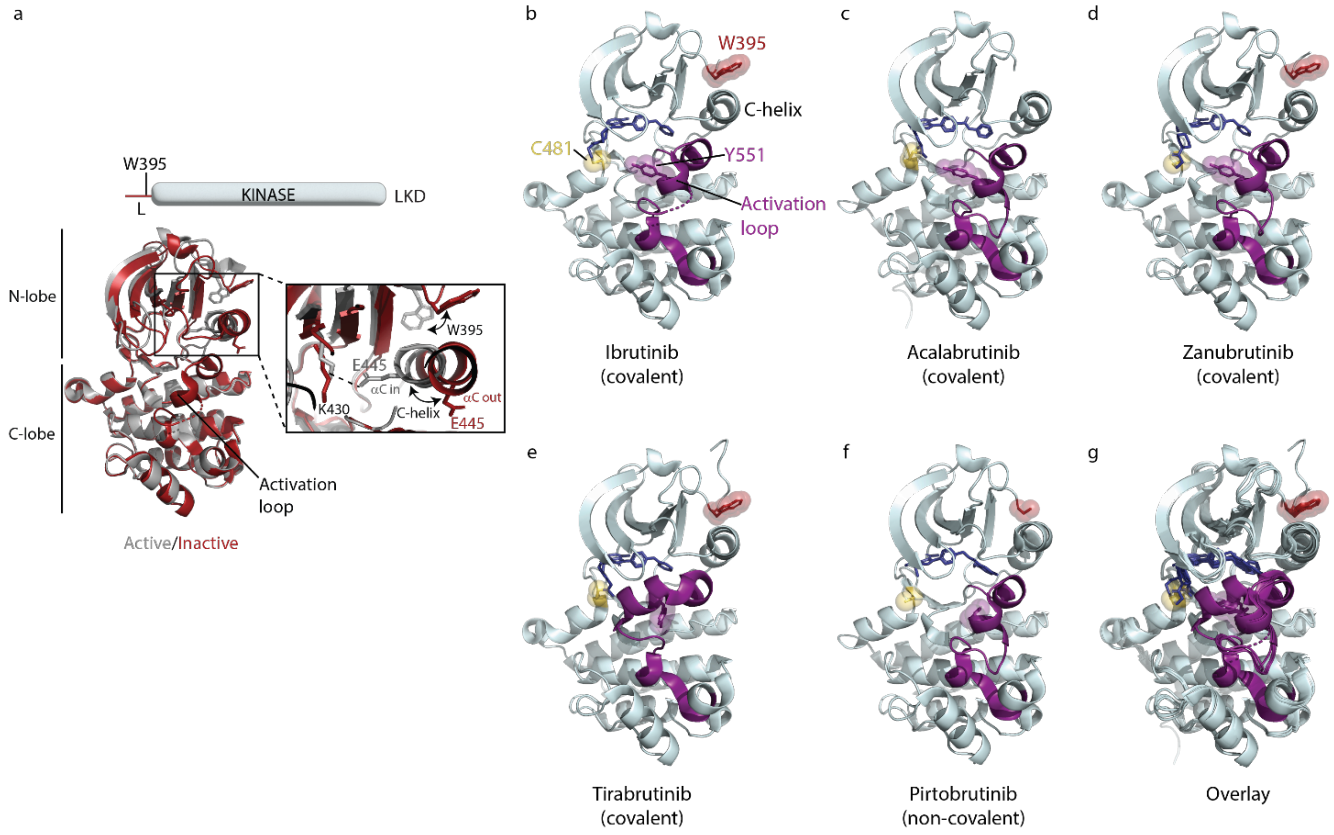

827

828

829 Figure 2: The BTK kinase domain can interconvert between active and inactive conformations. (a)
830 Superposition of the structure of BTK linker-kinase domain (LKD) bound to Dasatinib (PDB ID:
831 3K54) in the active kinase conformation (grey cartoon) with the Ibrutinib bound structure (PDB
832 ID: 5P9J) in the inactive conformation (red cartoon). The expanded inset shows the inward
833 movement of the αC-helix, the change in W395 rotamer conformation and the K430/E445 salt
834 bridge formation that accompanies kinase activation. (b-f) Co-crystal structures of BTK LKD
835 (light cyan cartoon) bound to Ibrutinib (PDB ID: 5P9J), Acalabrutinib (PDB ID: 8FD9),
836 Zanubrutinib (PDB ID: 6J6M), Tirabrutinib (PDB ID: 5P9M) and Pirtobrutinib (PDB ID: 8FLL)
837 in the inactive kinase conformation. The inhibitors are shown as dark blue sticks, the kinase

activation loop is purple and C481, Y551 and W395 residues are shown as sticks with transparent spheres. Electron density for part of the activation loop is missing in the Ibrutinib co-crystal structure and is indicated as dotted lines (b). In the Acalabrutinib structure, the activation loop has several mutations [36] and the SH2-kinase linker (including W395) is absent (c). Electron density for W395 sidechain is missing in the BTK:Pirtobrutinib co-crystal structure (f). (g) Overlay of the BTK:Ibrutinib, Acalabrutinib, Zanubrutinib, Tirabrutinib and Pirtobrutinib co-crystal structures. With the exception of the Tirabrutinib co-crystal structure (e), no major structural variation is observed in the kinase domains. The activation loop in the Tirabrutinib bound structure adopts a different conformation compared to the other co-crystal structures.

858 Figure 3:

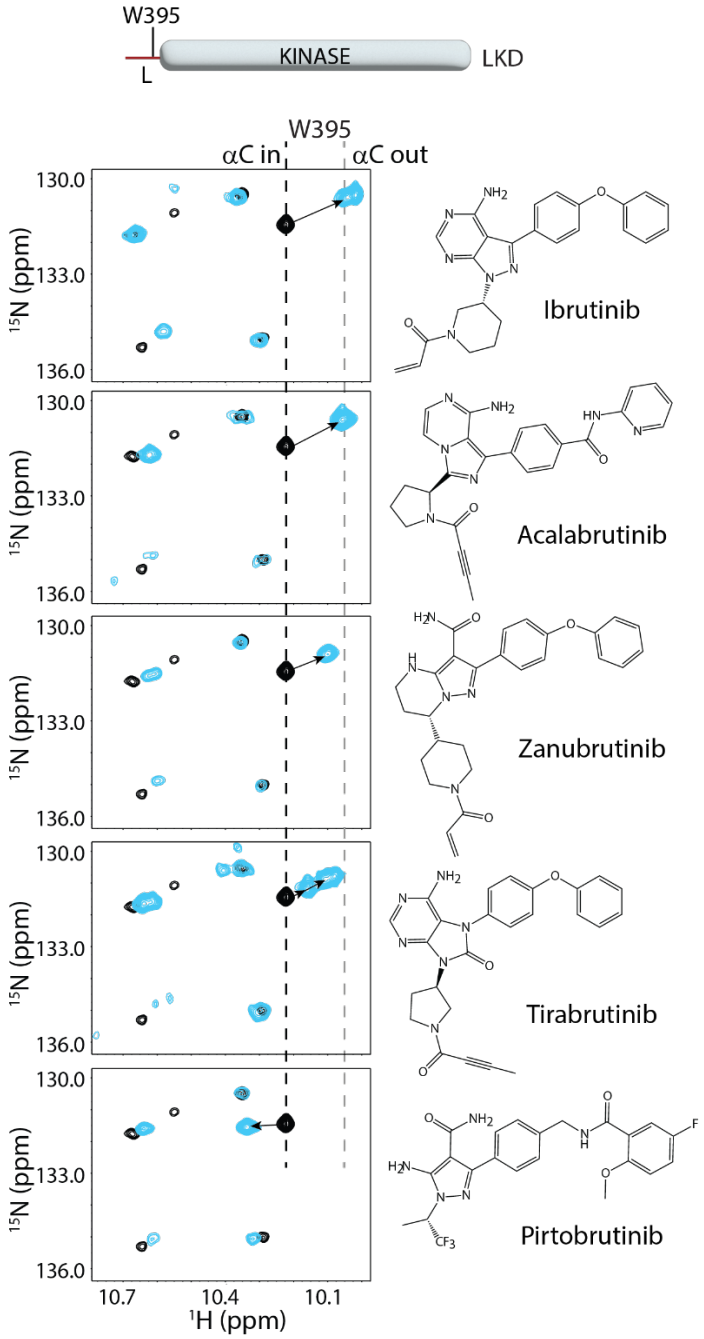

859

860

861 Figure 3: BTK inhibitors stabilize the inactive kinase conformation in solution. The tryptophan

862 side chain region of the ^{1}H-^{15}N TROSY HSQC spectra of ^{15}N-labelled apo BTK linker-kinase

863 domain (black spectrum) overlaid with that of the inhibitor bound spectrum (cyan spectrum). Here
864 and in subsequent figures, the broken black and grey lines indicate the position of the BTK W395
865 resonance in the active (αC-in) and inactive (αC-out) states respectively as shown in Figure 2a.
866 The shift in the BTK W395 resonance upon inhibitor binding is indicated by an arrow in each
867 spectrum. The structures of each inhibitor are shown on the right. The BTK W395 indole NH
868 resonance is in the inactive (αC-out) position in the Ibrutinib (published earlier [16]),
869 Acalabrutinib, Zanubrutinib and Tirabrutinib bound BTK LKD samples. Multiple peaks
870 corresponding to W395 are seen in the Tirabrutinib bound spectrum suggesting that the kinase
871 adopts multiple conformations in solution. The downfield shift observed in W395 in the
872 Pirtobrutinib bound structure is likely due to local changes in the chemical environment due to the
873 distinct chemical structure of Pirtobrutinib. W395 assignments in the inhibitor bound spectra were
874 confirmed by acquiring inhibitor bound spectra with the BTK LKD W395A mutant (see Supp.
875 Fig. S1).

876

877

878

879

880

881

882

883

Figure 4:

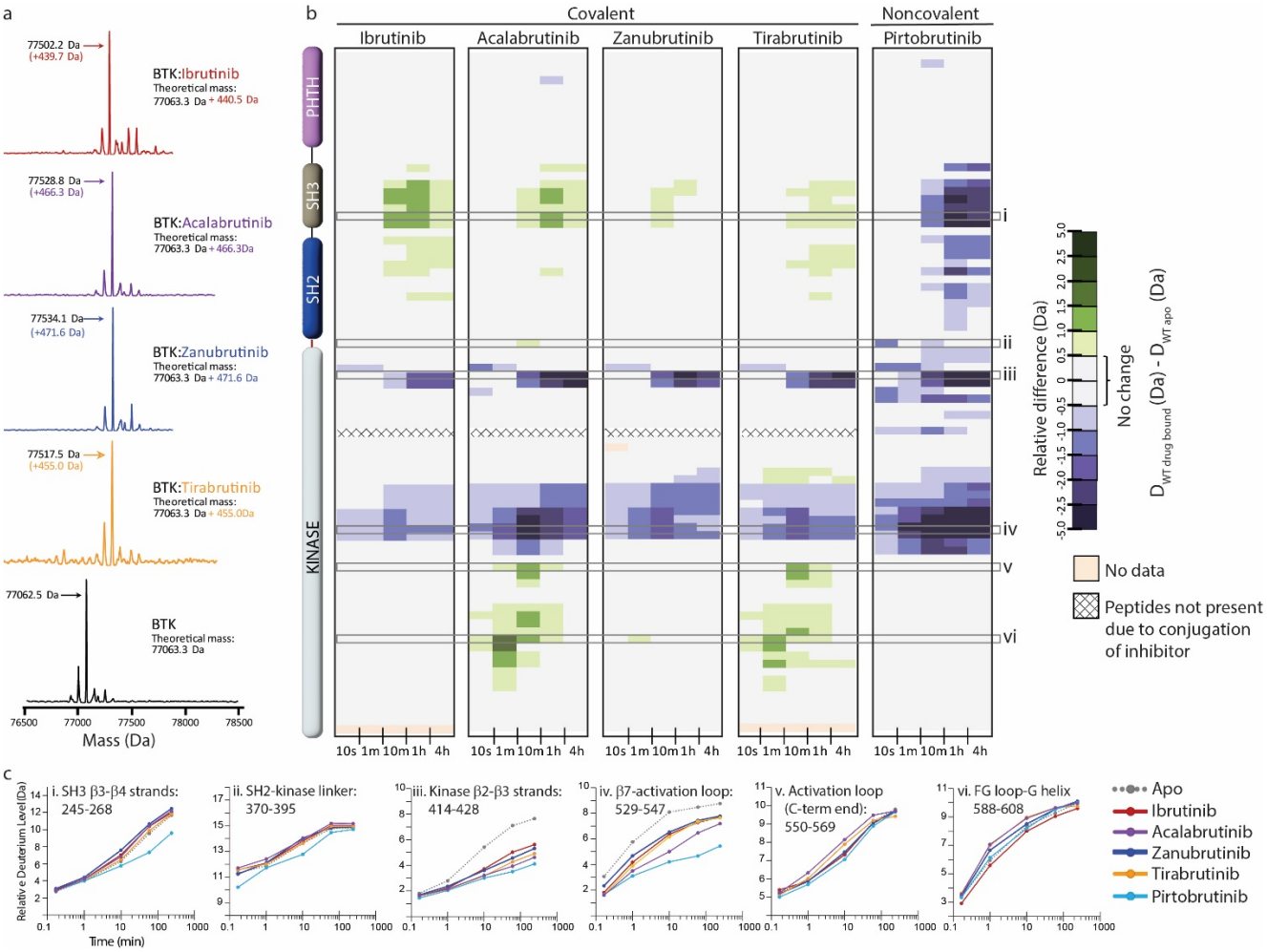

Figure 4: Assessing the impact of BTK inhibitors on full-length BTK by HDX-MS. (a) Intact mass analysis of wild-type FL BTK before (bottom spectrum, black) and after one hour incubation with a 2-fold molar excess of covalent BTK inhibitors: Ibrutinib (red), Acalabrutinib (purple), Zanubrutinib (blue) and Tirabrutinib (orange) show a mass increase of one inhibitor molecule. (b) Clinically approved BTK inhibitors induce allosteric changes in full-length BTK. Relative deuterium level of peptides in apo BTK was subtracted from the deuterium level of the corresponding peptide from each drug-bound form of BTK ($D_{WT\ drug\text{-}bound}$-$D_{WT\ apo}$) and the

894 differences colored according to the scale shown. In this and subsequent figures, peptic peptides
895 are shown from N- to C-terminus, top to bottom, and the amount of time in deuterium is shown
896 left to right. The relative difference data shown here represents a curated set of peptides that are
897 coincident across all 6 states (apo and five drug-bound BTK forms). The identification of these
898 chosen peptides, the relative difference values, and the complete data set for each state can be
899 found in the Supplemental Datafile. The approximate position of the domains of BTK, as described
900 in Figure 1a, is shown at the left. Deuterium incorporation curves of selected peptides (indicated
901 with a gray box in panel b and labelled i-vi) from various regions of the protein are shown below.
902 Data for Ibrutinib has been previously published [16].

903

904

905

906

907

908

909

910

911

912

913

914 Figure 5:

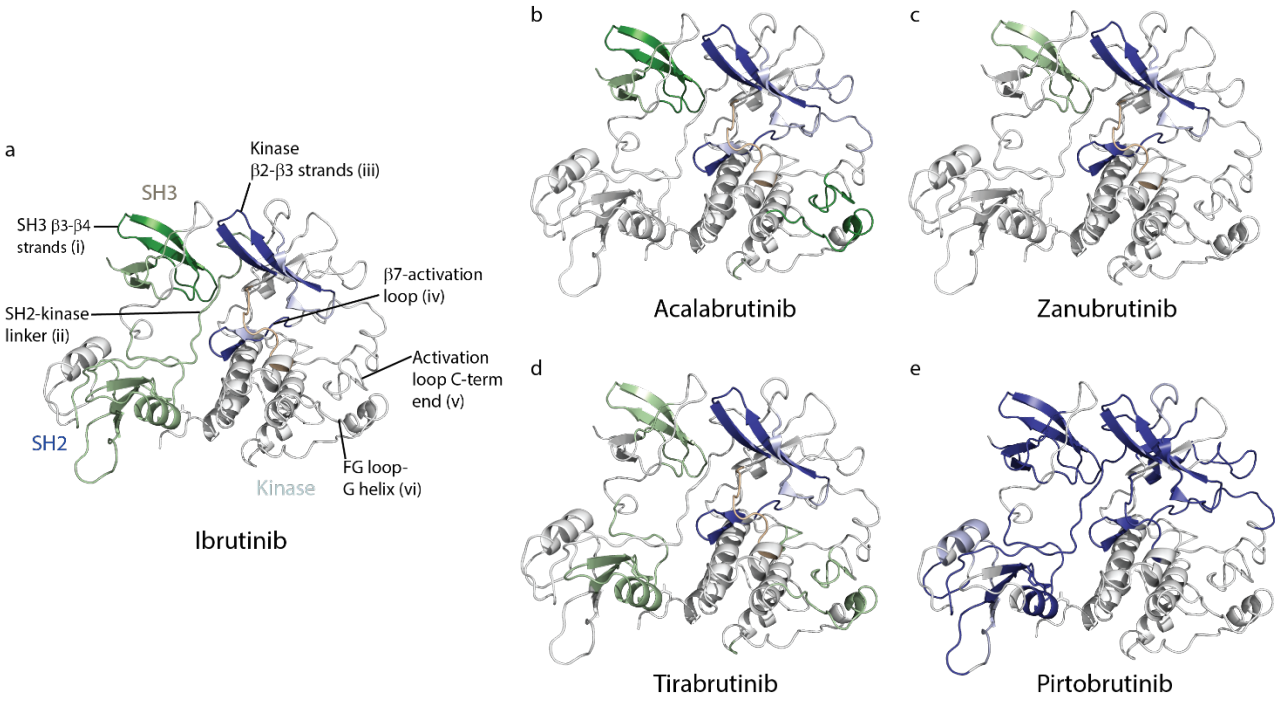

915

916

917 Figure 5: (a-e) Mapping the HDX-MS changes induced by each BTK inhibitor on the structure of
918 the BTK SH3-SH2-kinase fragment (PDB ID: 4XI2). Major differences greater than 1.0 Da are
919 shown as dark blue (decrease) or dark green (increase); modest differences between 0.5 Da and
920 1.0 Da are shown as light blue (decrease) and light green (increase). Localization of the changes
921 in deuterium incorporation was accomplished using overlapping peptides included in the complete
922 peptide data set provided in the Supplemental Datafile. The location of peptides i – vi from Figure
923 4 are indicated in panel a. Data corresponding to Ibrutinib has been previously published [16].

924

925

926 Figure 6:

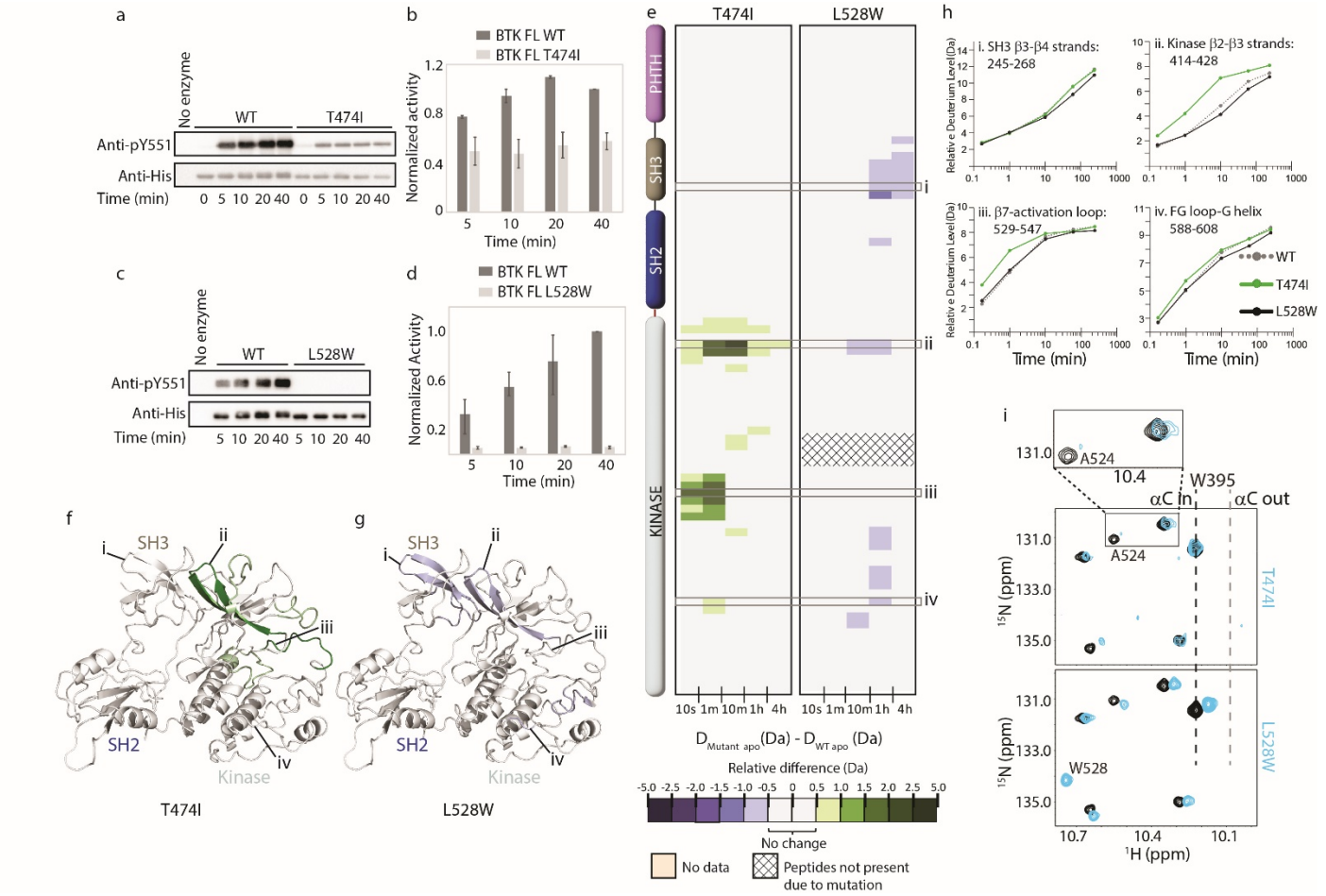

927

928 Figure 6: Probing the impact of the BTK resistance mutations T474I and L528W on BTK. (a-d)
929 Western blot comparing the kinase activity of full-length (FL) BTK wild-type (WT), T474I and
930 L528W mutants. BTK autophosphorylation was monitored using the BTK pY551 antibody and
931 the total protein levels monitored using the Anti-His antibody. (b, d) Histogram quantifying the
932 western blots shown in (a and c). The blots were quantified and normalized as described in the
933 Materials and Methods. Data shown are the average of three independent experiments. (e) HDX
934 difference data for the BTK T474I and L528W mutants ($D_{Mutant\ apo}$ -$D_{WT\ apo}$). Color scale and
935 peptide/time course arrangement are the same as in Figure 4. See the Supplemental Datafile for
936 additional information, including all peptide identifications and deuterium values. (f,g) Mapping

937 the mutational induced HDX-MS changes on the structure of the BTK SH3-SH2-kinase fragment.
938 (h) Deuterium incorporation curves of selected peptides (indicated with a gray box in panel e and
939 labelled i-iv) from various regions of the protein are shown. (i) The tryptophan side chain region
940 of the ^{1}H-^{15}N TROSY HSQC spectra of ^{15}N-labelled apo WT BTK linker-kinase domain (black
941 spectrum) overlaid with that of the apo mutant kinase spectrum (cyan spectrum). The boxed region
942 in the T474I spectral overlay is expanded above.

943

944

945

946

947

948

949

950

951

952

953

954

955

956 Figure 7:

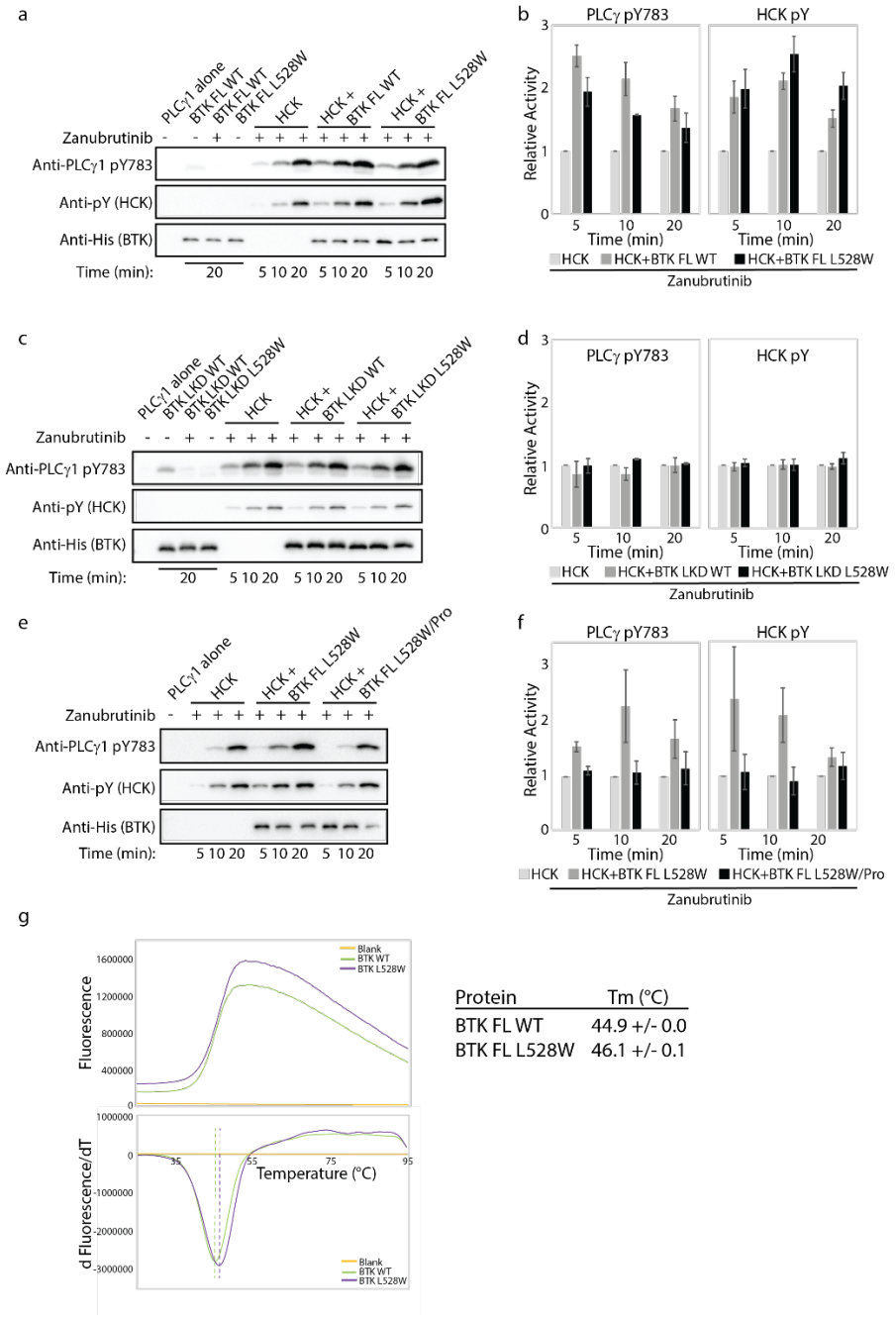

Protein	Tm (°C)
BTK FL WT	44.9 +/- 0.0
BTK FL L528W	46.1 +/- 0.1

957

958

959 Figure 7: The BTK L528W mutant can activate HCK. (a-f) Kinase activity of HCK in the presence

960 or absence of full-length BTK L528W mutant was compared in a western blot assay by monitoring

961 PLCγ1 phosphorylation (pY783 antibody) and HCK autophosphorylation (pY antibody). Total
962 protein levels monitored using the Anti-His antibody. Full-length WT BTK preincubated with
963 Zanubrutinib was used as a control. (b, d and f) Histogram quantifying the western blots shown in
964 (a, c and e). The blots were quantified and normalized as described in the Materials and Methods.
965 Data shown are the average of three independent experiments. (b and c) Kinase activity of HCK
966 in the presence or absence of the isolated linker kinase domain (LKD) fragment of the BTK L528W
967 mutant (b) or the full-length proline mutant of BTK L528W (BTK FL L528W/Pro: BTK L528W/
968 P189A/P192A/P203A/P206A, (c)) was compared as in (a). (g) Thermal stability analysis of BTK
969 FL WT and BTK FL L528W. Data shown are the average of three independent experiments.

970

971

972

973

974

975

976

977

978

979

980

Figure 8:

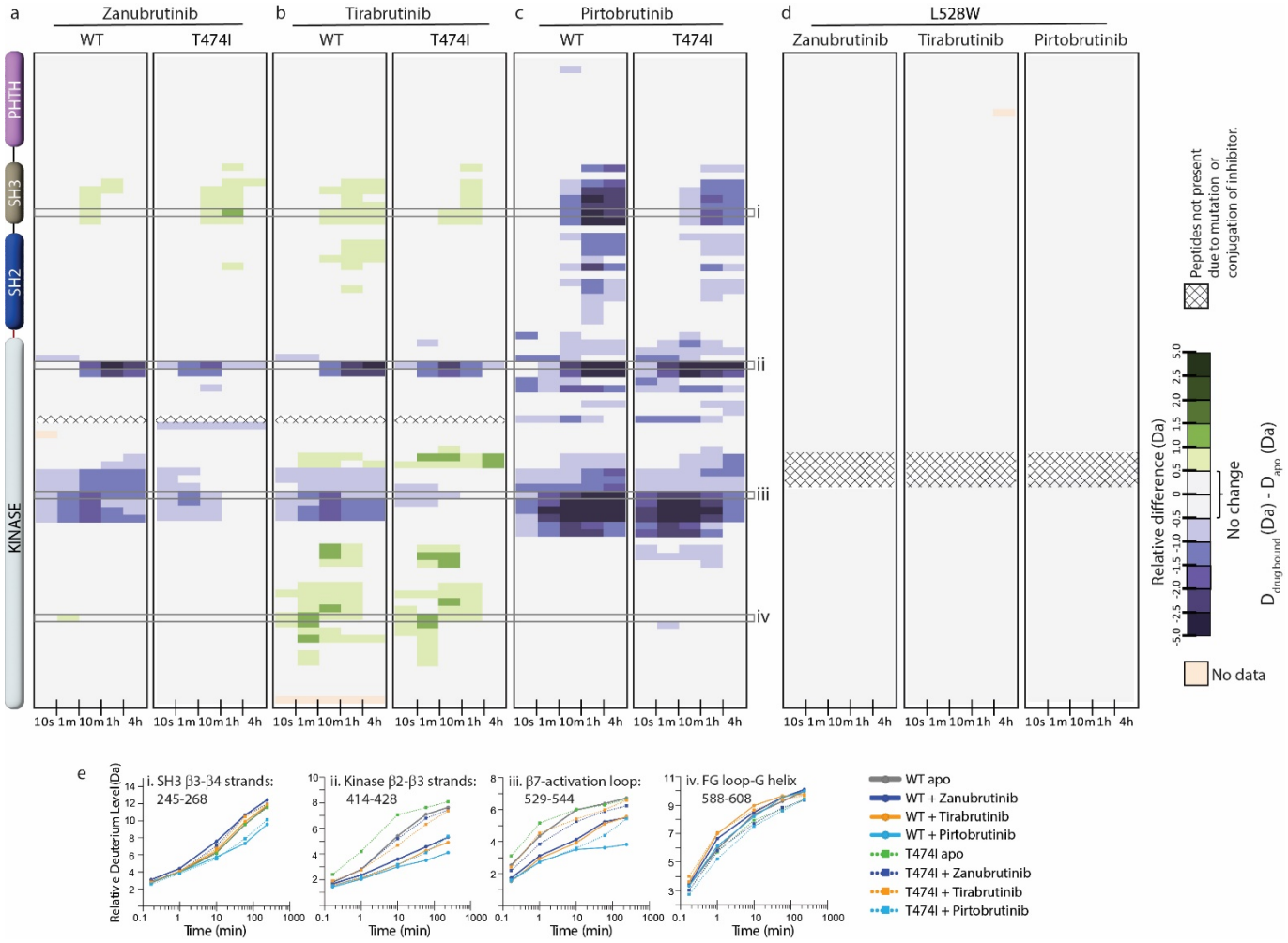

Figure 8: HDX-MS analysis of BTK inhibitor binding to BTK T474I and L528W mutants. (a-d) Relative deuterium level of peptides in apo mutant BTK was subtracted from the deuterium level of the corresponding peptide from each inhibitor-bound form of BTK ($D_{drug\text{-}bound}$-D_{apo}) and compared to the changes in the WT protein. The differences are colored according to the scale shown. (e) Deuterium incorporation curves of selected peptides (indicated with a gray box in panels a-c, and labelled i-iv) are shown.

990 Figure 9:

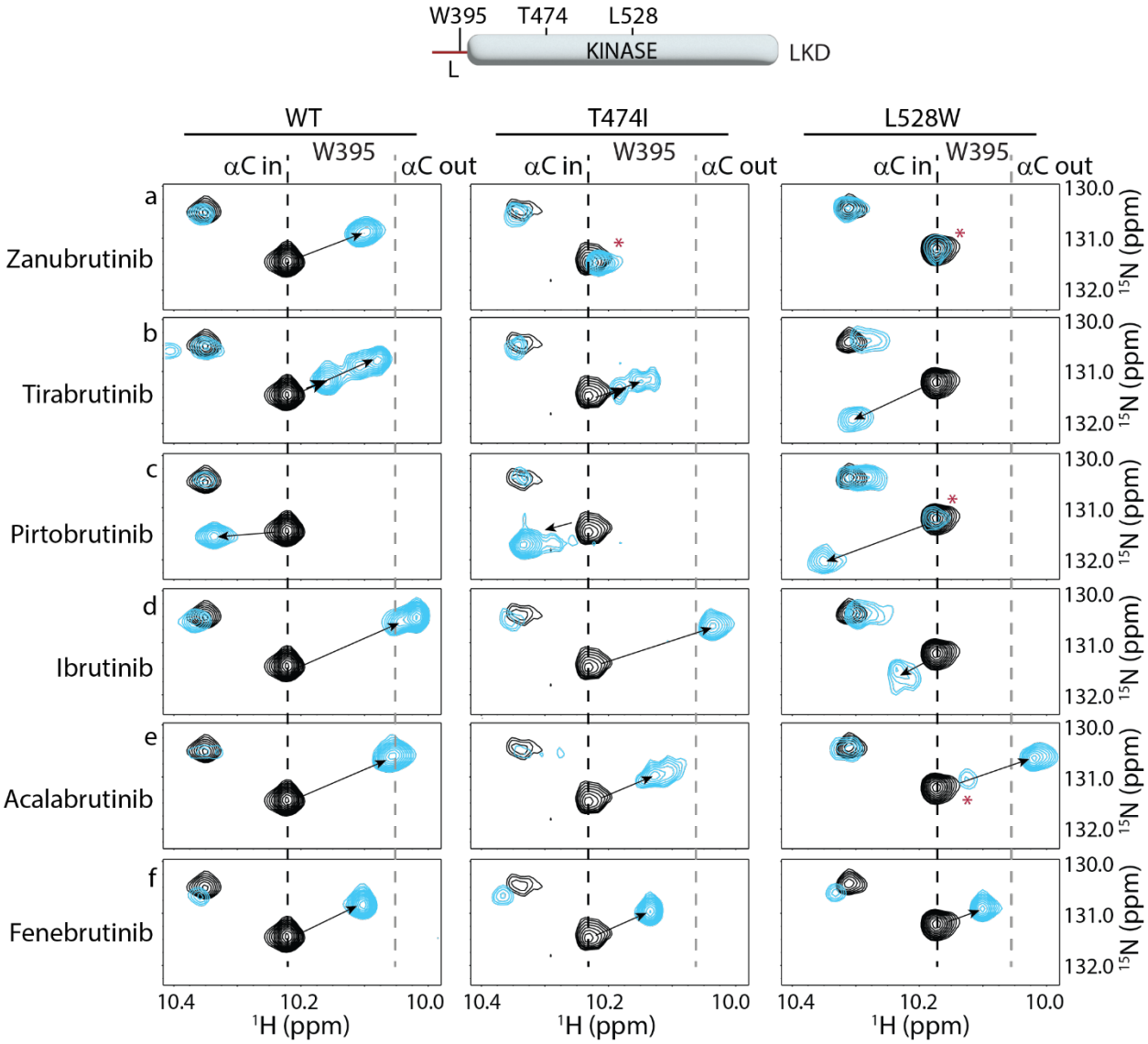

991

992

993 Figure 9: NMR analysis of BTK inhibitor binding to the BTK T474I and L528W mutants. The
994 tryptophan side chain region of the ^{1}H-^{15}N TROSY HSQC spectra of ^{15}N-labelled apo BTK linker-
995 kinase domain (black spectrum) overlaid with that of the inhibitor bound spectrum (cyan
996 spectrum). The broken black and grey lines indicate the position of the BTK W395 resonance and
997 have been described earlier in Figure 3. The shift in the BTK W395 indole NH resonance upon

998 inhibitor binding is indicated by an arrow in each spectrum. The red asterisks indicate the presence
999 of unbound kinase domain in the inhibitor bound NMR sample.

1000

1001 TABLES

1002 **Table 1**: Half-life of clinically approved BTK inhibitors: Ibrutinib[64], Acalabrutinib [65],
1003 Zanubrutinib [66], Tirabrutinib [67] and Pirtobrutinib [68].

Inhibitor	Half life (h)
Ibrutinib	2 - 3
Acalabrutinib	0.6 - 2.8
Zanubrutinib	4
Tirabrutinib	6.5 - 8
Pirtobrutinib	20

1004

1005

1006

1007

1008

1009

1010

1011

1012

1013

1014 Supp. Fig. S1

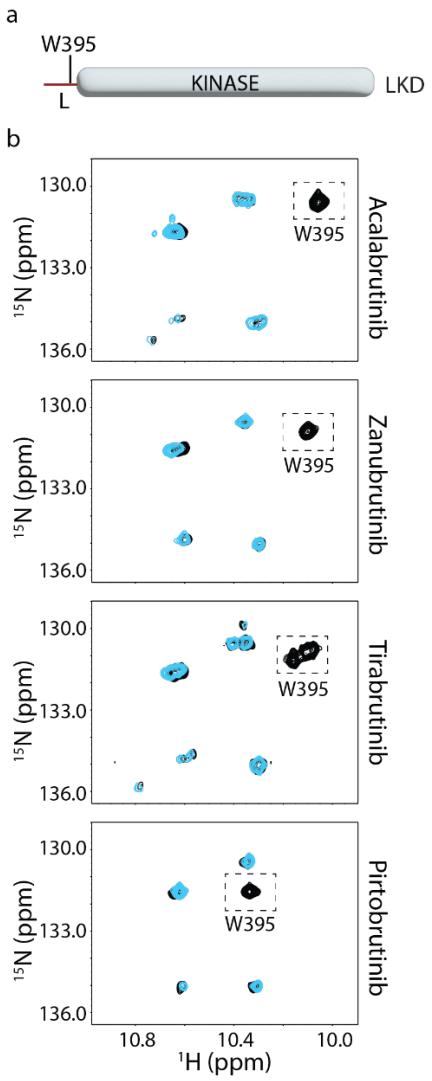

1015

1016

1017 Supp Fig. S1: Assignment of W395 in inhibitor bound spectra of BTK LKD. The tryptophan side

1018 chain region of the ^{1}H-^{15}N TROSY HSQC spectra of ^{15}N-labelled inhibitor bound BTK linker-

1019 kinase domain WT (black spectrum) overlaid with that of the inhibitor bound BTK LKD W395A

1020 spectrum (cyan spectrum). The boxed peak indicates the W395 resonance in each of the WT

1021 inhibitor bound spectrum.

1022 Supplemental Datafile:

1023 Microsoft Excel file providing enhanced experimental details for HDX-MS including minimum
1024 criteria specified by [61], lists of all peptides by residue number, sequence, as well as deuterium
1025 levels measured for each Figure. The value of each deuterium difference for every colored box in
1026 each Figure as well as the complete dataset for each state are also found in this file.

1027

1028 **Supp. Table 1**: BTK mutations detected in CLL patients treated with BTK inhibitors. In addition
1029 to mutations in BTK C481, T474 and L528, other BTK mutations that have been detected include:
1030 R28S, E108K, G164D, V416L, A428D, M437R, R490H, Q516K, V537I and T316A [21-24, 26-
1031 30, 32-34].

BTK inhibitor	Total number of patients with BTK mutations.	Patients with BTK C481 mutated.	Patients with BTK T474 mutated.	Patients with BTK L528 mutated.	Patients with other BTK mutations.
Ibrutinib	106	95 (90%)	1 (1%)	1 (1%)	5 (5%)
Acalabrutinib	11	11 (100%)	1 (9%)	0	0
Zanubrutinib	17	15 (88%)	0	11 (65%)	0
Tirabrutinib	6	4 (67%)	3 (50%)	4 (67%)	1 (17%)
Pirtobrutinib	9	0	2 (22%)	4 (44%)	3 (33%)

1032